

CHAPTER 4. ANALYSIS AND DESIGN OF SINGLE-MODE FIBER WITH ZERO POLARIZATION-MODE DISPERSION

Polarization-mode dispersion (PMD) has gained considerable attention over the past few years. It has been the subject of many experimental and theoretical investigations [104] in order to thoroughly understand its effects and identify the major sources contributing to this phenomenon. Interest in this subject lies upon surpassing the limitations caused by PMD in fibers, especially in long distance telecommunication systems. Such limitations are exhibited in bandwidth-distance product, bit-rate, pulse width distortion, power penalty in the receiver, and nonlinear distortions in analog systems.

4.1 POLARIZATION-MODE DISPERSION

It has been established that in general, two factors contribute to polarization-mode dispersion (PMD) in circular fibers: the deformation of the circular geometry and the internal stresses which leads to stress anisotropy. Both effects occur during the manufacturing process. In this chapter, the investigation of PMD is limited to elliptical deformation of fibers.

For a deformed fiber with small core ellipticity, the fundamental LP_{01} mode splits into two orthogonally polarized modes with slightly different propagation constants of these two modes. The amount of PMD in fibers depends on the difference between the propagation constants. In ordinary step-index single-mode fibers, PMD vanishes outside the single-mode wavelength region [106]. In other words, at the wavelength of zero PMD two or more modes are supported by the fiber, thus significant signal distortion occurs due to modal dispersion effect. To improve fiber performance in long-haul high bit rate systems, a zero PMD must occur in the single-mode wavelength region. Few methods for canceling out the polarization mode dispersion have been proposed by researchers. Also, it has been verified experimentally that low PMD due to form-induced and stress-induced

birefringence can be achieved for short-length PMD (measured in ps/km) by partial cancellation of the two induced effects, [107].

The main goal in this chapter is to design a fiber that provides zero PMD in a single-mode region. A fiber design with depressed core and multiple claddings are promising for this purpose. The approach adopted in examining this fiber is based on the analysis of a single-mode fiber with small ellipticity. Then the analysis results are used to design a fiber with zero or very small PMD at the wavelength of operation. In addition to requiring zero PMD, other critical fiber properties such as effective area, mode field diameter, field distribution, and chromatic dispersion will also be examined.

4.2 SINGLE-MODE FIBERS WITH SMALL ELLIPTICITY

4.2.1 Analysis of Slightly Elliptical Multiple-Clad Fiber

The analysis of slightly elliptical multiple clad fibers is presented using a perturbation technique. Fields are expressed in power series of ellipticity factor ϵ , and only the zero and first order terms are retained in the solutions. Propagation properties, including birefringence, effective area, mode-field diameter, and dispersion are presented for an example design.

4.2.1.1 Field Solutions

Let us consider an N layers optical fiber consisting of a central core region and several claddings, with boundaries of every two neighboring layers being slightly elliptical. Each layer is assumed to be isotropic, homogeneous, lossless, and linear. The i th layer, with $i = 1$ representing the core and $i > 1$ referring to the cladding regions, is characterized by a radius r_i and refractive index n_i , where $i = 1, 2, \dots, N$. The outer cladding layer is assumed to extend to infinity in the radial direction because the field of guided modes decay exponentially in the radial direction in this cladding. Figure 4.1 illustrates the cross

sectional view of such multiple clad fiber. The boundary between the i th and $(i+1)$ th layers is described by

$$r_i = \alpha_i [1 + e \cos(2\varphi)] \quad (4.1)$$

where e is the ellipticity factor and φ is the azimuthal angle measured from the x -axis. The semi-major and semi-minor axis are $\alpha_i (1 + e)$ and $\alpha_i (1 - e)$, respectively, for the i th elliptical boundary. For a perfectly circular fiber, the ellipticity factor $e = 0$ and the layers' radii become $r_i = \alpha_i$.

For the fundamental LP_{01} mode, the scalar fields solutions are expressed as

$$\psi_i(r, \varphi) = f_{0i}(r) + e f_{1i}(r, \varphi) + O(e^2); \quad i = 1, 2, \dots, N \quad (4.2)$$

where $f_{0i}(r)$ is the zero-order solution and is the same as that if the fiber were circular. That is,

$$f_{0i}(r) = A_i Z_{0i}(u_i r) + B_i \bar{Z}_{0i}(u_i r) \quad (4.3)$$

where

$$Z_{0i} = \begin{cases} J_0, & \bar{\beta}_0 < n_i \\ I_0, & \bar{\beta}_0 > n_i \end{cases} \quad (4.4)$$

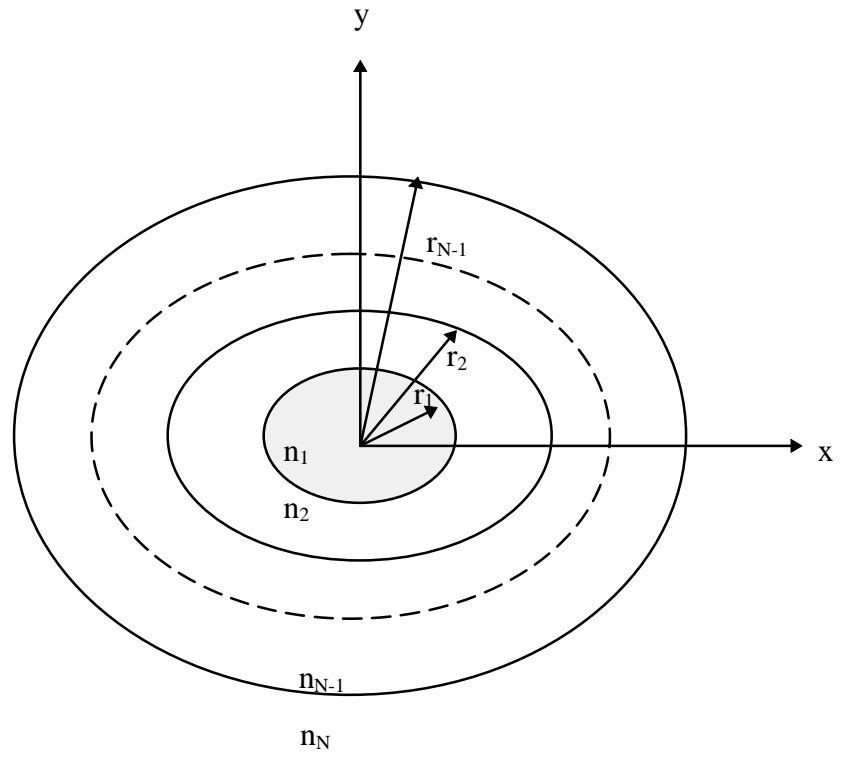


Figure 4.1 Cross section view of multiple-clad elliptical fiber consisting of N layers.

$$\bar{Z}_{0i} = \begin{cases} Y_0, \bar{\beta}_0 < n_i \\ K_0, \bar{\beta}_0 > n_i \end{cases} \quad (4.5)$$

and

$$u_i = (2\pi/\lambda) (|n_i^2 - \bar{\beta}_0^2|)^{1/2} \quad (4.6)$$

with $\bar{\beta}_0 = \beta_0/(2\pi/\lambda)$. In (4.4) and (4.5), J_0 and Y_0 are the zero-order Bessel functions of the first and second kinds, while I_0 and K_0 are the zero-order modified Bessel functions of the first and second kinds, respectively. In order for the solution in (4.3) to be finite at $r = 0$ and $r = \infty$, it is necessary that $B_1 = A_N = 0$.

For the case of ordinary step-index fibers, where $N = 2$, it has been established that in order to satisfy boundary conditions at $r = a [1 + \cos(2\phi)]$, the function $f_{1i}(r, \phi)$ should assume the form $g(r)\cos(2\phi)$, where $g(r)$ is the solution of Bessel differential equation of order 2. Clearly, the same property holds for multiple clad fibers. Thus, the solution for $f_{1i}(r, \phi)$ can be written as

$$f_{1i}(r, \phi) = \hat{f}_{1i}(r) \cos(2\phi) \quad (4.7a)$$

$$\hat{f}_{1i}(r) = [C_i Z_{2i}(u_i r) + D_i \bar{Z}_{2i}(u_i r)] \quad (4.7b)$$

where Z_{2i} and \bar{Z}_{2i} follow the same definition as those for Z_{0i} and \bar{Z}_{0i} , but with subscript zero replaced with 2, and C_i and D_i are constant coefficients.

4.2.1.2 Boundary Conditions

The fields $\psi_i(r, \phi)$ and their derivatives $\partial \psi_i(r, \phi)/\partial r$ must be continuous at the boundaries $r = r_i$. Implementing these conditions results in the following equation,

$$f_{0i} [\alpha_i (1 + \text{ecos}(2\varphi))] + e \hat{f}_{1i}(r) [\alpha_i (1 + \text{ecos}(2\varphi))] \cos(2\varphi) = f_{0,i+1} [\alpha_i (1 + \text{ecos}(2\varphi))] + e \hat{f}_{1,i+1}(r) [\alpha_i (1 + \text{ecos}(2\varphi))] \cos(2\varphi), \quad (4.8a)$$

and

$$f'_{0i} [\alpha_i (1 + \text{ecos}(2\varphi))] + e \hat{f}'_{1i} [\alpha_i (1 + \text{ecos}(2\varphi))] \cos(2\varphi) = f'_{0,i+1} [\alpha_i (1 + \text{ecos}(2\varphi))] + e \hat{f}'_{1,i+1} [\alpha_i (1 + \text{ecos}(2\varphi))] \cos(2\varphi) \quad (4.8b)$$

Next, we obtain Taylor series expansions of the functions f_{0i} , f'_{0i} , $f_{0,i+1}$, $f'_{0,i+1}$, \hat{f}'_{1i} , $\hat{f}'_{1,i+1}$, using the following relationship,

$$f[\alpha_i (1 + \text{ecos}(2\varphi))] = f(\alpha_i) + e [\alpha_i \cos(2\varphi) f'(\alpha_i)] + 0(e^2) \quad (4.9a)$$

$$f'[\alpha_i (1 + \text{ecos}(2\varphi))] = f'(\alpha_i) + e [\alpha_i \cos(2\varphi) f''(\alpha_i)] + 0(e^2) \quad (4.9b)$$

where $f = f_{0i}$, $f_{0,i+1}$, \hat{f}_{1i} , $\hat{f}_{1,i+1}$ and $f' = f'_{0i}$, $f'_{0,i+1}$, \hat{f}'_{1i} , $\hat{f}'_{1,i+1}$

Using (4.9) in (4.8) and collecting terms of $0(e^0)$, $0(e^1)$, $0(e^2)$, ..., we obtain

$$[f_{0i}(\alpha_i) - f_{0,i+1}(\alpha_i)] + e \{ [f'_{0i}(\alpha_i) - f'_{0,i+1}(\alpha_i)] \alpha_i + \hat{f}_{1i}(\alpha_i) - \hat{f}_{1,i+1}(\alpha_i) \} \cos(2\varphi) + 0(e^2) = 0 \quad (4.10a)$$

$$[f'_{0i}(\alpha_i) - f'_{0,i+1}(\alpha_i)] + e \{ [f''_{0i}(\alpha_i) - f''_{0,i+1}(\alpha_i)] \alpha_i + \hat{f}'_{1i}(\alpha_i) - \hat{f}'_{1,i+1}(\alpha_i) \} \cos(2\varphi) + 0(e^2) = 0 \quad (4.10b)$$

Equating the coefficients of $0(e^0)$, $0(e^1)$, ..., terms, (4.10a) and (4.10b) reduce to

$$f_{0i}(\alpha_i) - f_{0,i+1}(\alpha_i) = 0 \quad (4.11)$$

$$f'_{0i}(\alpha_i) - f'_{0,i+1}(\alpha_i) = 0 \quad (4.12)$$

$$[f'_{0i}(\alpha_i) - f'_{0,i+1}(\alpha_i)] \alpha_i + \hat{f}_{1i}(\alpha_i) - \hat{f}_{1,i+1}(\alpha_i) = 0 \quad (4.13)$$

$$[f''_{0i}(\alpha_i) - f''_{0,i+1}(\alpha_i)] \alpha_i + \hat{f}'_{1i}(\alpha_i) - \hat{f}'_{1,i+1}(\alpha_i) = 0 \quad (4.14)$$

The propagation constant β_o as well as the coefficients A_i and B_i in (4.3) can be determined from (4.11) and (4.12) in terms of one coefficient, e.g. A_i . Equations (4.13) and (4.14) in conjunction with (4.12) reduce to

$$\hat{f}_{1i}(\alpha_i) - \hat{f}_{1,i+1}(\alpha_i) = 0 \quad (4.15)$$

$$\hat{f}'_{1i}(\alpha_i) - \hat{f}'_{1,i+1}(\alpha_i) = -\alpha_i [f''_{0i}(\alpha_i) - f''_{0,i+1}(\alpha_i)] \quad (4.16)$$

From (4.15) and (4.16) the rest of the coefficients, C_i and D_i , can be found in terms of A_i .

4.2.2 Analysis of Four-Layers Fiber

4.2.2.1 Field Solutions and Characteristic Equations

The general results derived in the previous sub-sections will be used to find the field solutions, characteristic equation, and ultimately birefringence. From (4.3) and (4.7), the field solutions are expressed as

$$f_{0i}(r) = \begin{cases} A_1 Z_{01}(u_1 r), & r < a_1 \\ A_2 Z_{02}(u_2 r) + B_2 \bar{Z}_{02}(u_2 r), & a_1 < r < a_2 \\ A_3 Z_{03}(u_3 r) + B_3 \bar{Z}_{03}(u_3 r), & a_2 < r < a_3 \\ B_4 \bar{Z}_{04}(u_4 r), & r > a_3 \end{cases} \quad (4.29)$$

$$\hat{f}_{1i}(r) = \begin{cases} C_1 Z_{21}(u_1 r), & r < a_1 \\ C_2 Z_{22}(u_2 r) + D_2 \bar{Z}_{22}(u_2 r), & a_1 < r < a_2 \\ C_3 Z_{23}(u_3 r) + D_3 \bar{Z}_{23}(u_3 r), & a_2 < r < a_3 \\ D_4 \bar{Z}_{24}(u_4 r), & r > a_3 \end{cases} \quad (4.30)$$

The characteristic equation and the amplitude coefficients are determined using (4.29) in applying the boundary conditions stated in (4.11) and (4.12). The results are expressed as

$$\xi_2 \frac{(\eta_{10} - \eta_9)}{(\eta_{10} - \eta_8)} = \frac{(\eta_1 - \eta_3)(\eta_4 - \eta_7) - \xi_1(\eta_1 - \eta_2)(\eta_5 - \eta_7)}{(\eta_1 - \eta_3)(\eta_4 - \eta_6) - \xi_1(\eta_1 - \eta_2)(\eta_5 - \eta_6)} \quad (4.31)$$

where the η_j ; $j = 1, 2, \dots, 10$, ξ_1 and ξ_2 are defined in Appendix A.

4.2.2.2 Amplitude Coefficients

The amplitude coefficients are determined in terms of A_1 as

$$A_2 = \frac{Z_{01}(U_1)}{Z_{02}(U_2)} \cdot \frac{(\eta_1 - \eta_3)}{(\eta_2 - \eta_3)} \cdot A_1$$

$$B_2 = \frac{Z_{01}(U_1)}{\bar{Z}_{02}(U_2)} \cdot \frac{(\eta_1 - \eta_2)}{(\eta_3 - \eta_2)} \cdot A_1$$

$$A_3 = \frac{Z_{02}(\bar{U}_2)}{Z_{03}(U_3)} \cdot \frac{(\eta_7 - \eta_4)}{(\eta_7 - \eta_6)} \cdot A_2 + \frac{\bar{Z}_{02}(\bar{U}_2)}{Z_{03}(U_3)} \cdot \frac{(\eta_7 - \eta_5)}{(\eta_7 - \eta_6)} \cdot B_2$$

$$B_3 = \frac{Z_{02}(\bar{U}_2)}{\bar{Z}_{03}(U_3)} \cdot \frac{(\eta_6 - \eta_4)}{(\eta_6 - \eta_7)} \cdot A_2 + \frac{\bar{Z}_{02}(\bar{U}_2)}{\bar{Z}_{03}(U_3)} \cdot \frac{(\eta_6 - \eta_5)}{(\eta_6 - \eta_7)} \cdot B_2$$

$$\mathbf{B}_4 = \frac{\mathbf{Z}_{03}(\bar{\mathbf{U}}_3)}{\bar{\mathbf{Z}}_{04}(\mathbf{U}_4)} \cdot \mathbf{A}_3 + \frac{\bar{\mathbf{Z}}_{03}(\bar{\mathbf{U}}_3)}{\bar{\mathbf{Z}}_{04}(\mathbf{U}_4)} \cdot \mathbf{B}_3 \quad (4.32)$$

The rest of the amplitude coefficients, \mathbf{C}_k and \mathbf{D}_{k+1} where $k = 1, 2,$ and $3,$ are also determined in terms of \mathbf{A}_1 and are shown in Appendix A.

4.2.2.3 Birefringence Calculations

To calculate birefringence, first the difference between the scalar propagation constant $\tilde{\beta}$ and the exact (vector) propagation constant β is obtained from the following relationship [106]

$$\tilde{\beta}^2 - \beta^2 = \left(\int_S (\nabla_t \cdot \vec{e}_t) [\vec{e}_t \cdot \nabla_t (\ln n^2(r, \varphi))] ds \right) / \left(\int_S |\vec{e}_t|^2 ds \right) \quad (4.33)$$

where \vec{e}_t is $\psi \hat{a}_x$ or $\psi \hat{a}_y$ for x or y polarized fundamental LP_{01} modes, and S is the cross-section area of the fiber. Now, we need to calculate $\nabla_t (\ln n^2(r, \varphi))$,

$$\begin{aligned} \nabla_t (\ln n^2(r, \varphi)) &= [2 n(r, \varphi) [\partial n(r, \varphi) / \partial r] / n^2(r, \varphi)] \hat{a}_r + \\ & (1/r) 2 n(r, \varphi) [\partial n(r, \varphi) / \partial \varphi] / n^2(r, \varphi) \hat{a}_\varphi \\ &= 2 / n(r, \varphi) [[\partial n(r, \varphi) / \partial r] \hat{a}_r + [(1/r) \partial n(r, \varphi) / \partial \varphi] \hat{a}_\varphi] \\ &= 2 \nabla_t (n(r, \varphi)) / n(r, \varphi) \end{aligned}$$

In the case of a step-index profile, $n^2(r, \varphi)$ is constant in each region and only the index discontinuities at the boundaries contribute to $\nabla_t (\ln n^2(r, \varphi))$.

For the four-layer fiber under consideration in the design, we can write

$$\begin{aligned}\nabla_t (\ln n^2(r,\varphi)) &= 2 \left[\left(\frac{n_2-n_1}{n_1} \right) \delta[r - \alpha_1(1 + e\cos(2\varphi))] + \left(\frac{n_3-n_2}{n_2} \right) \delta[r - \alpha_2(1 + e\cos(2\varphi))] + \left(\frac{n_4-n_3}{n_3} \right) \delta[r - \alpha_3(1 + e\cos(2\varphi))] \right] (\hat{a}_r + 2e\sin(2\varphi)\hat{a}_\varphi) \\ &= g(r,\varphi)(\hat{a}_r + 2e\sin(2\varphi)\hat{a}_\varphi)\end{aligned}$$

The vector $\hat{a}_r + 2e\sin(2\varphi)\hat{a}_\varphi$ is, in fact, the gradient of $f(r,\varphi) = r - \alpha_i(1 + e\cos(2\varphi))$, as shown below

$$\begin{aligned}\nabla f(r,\varphi) &= \hat{a}_r + ((2\alpha_i e\sin(2\varphi))/r)\hat{a}_\varphi = \hat{a}_r + [(2\alpha_i e\sin(2\varphi))/\alpha_i(1 + e\cos(2\varphi))]\hat{a}_\varphi \\ &= \hat{a}_r + [(2e\sin(2\varphi))/(1 + e\cos(2\varphi))]\hat{a}_\varphi \cong \hat{a}_r + 2e\sin(2\varphi)(1 - e\cos(2\varphi))\hat{a}_\varphi \\ &\cong \hat{a}_r + 2e\sin(2\varphi) - 2e^2\sin(2\varphi)\cos(2\varphi)\hat{a}_\varphi \\ &\cong \hat{a}_r + 2e\sin(2\varphi)\hat{a}_\varphi\end{aligned}$$

The next step is to carry out the analysis for both polarizations x and y of the fundamental LP_{01} mode separately. For the LP_{01}^x mode we have

$$\begin{aligned}\vec{e}_t &= \psi(r,\varphi) \hat{a}_x = \psi(r,\varphi) [\cos(\varphi)\hat{a}_r - \sin(\varphi)\hat{a}_\varphi] \\ \nabla_t \cdot \vec{e}_t &= (1/r)(\partial/\partial r)(r e_r) + (1/r)(\partial e_\varphi/\partial \varphi)\end{aligned}$$

$$\begin{aligned}\psi(r,\varphi) &= f_0(r) + e f_1(r,\varphi) + O(e^2); \text{ where } f_1(r,\varphi) = \hat{f}_1(r) \cos(2\varphi), \text{ then} \\ (\nabla_t \cdot \vec{e}_t) [\vec{e}_t \cdot \nabla_t (\ln n^2(r,\varphi))] &\text{ becomes}\end{aligned}$$

$$\begin{aligned}
(\nabla_t \cdot \vec{e}_t)[\vec{e}_t \cdot \nabla_t (\ln n^2(r, \varphi))] &= [f'_0(r) \cos(\varphi) + e(\hat{f}'_1(r) \cos(\varphi) \cos(2\varphi) + \\
(2/r) \hat{f}_1 \sin(\varphi) \sin(2\varphi)] [f_0(r) + e \hat{f}_1(r) \cos(2\varphi)].g(r, \varphi) [\cos(\varphi) - 2e \sin(\varphi) \sin(2\varphi)] \\
&= g_x(r, \varphi)
\end{aligned}$$

For the LP₀₁^y mode we have

$$\vec{e}_t = \psi(r, \varphi) \hat{a}_y = \psi(r, \varphi) [\sin(\varphi) \hat{a}_r - \cos(\varphi) \hat{a}_\varphi]$$

To obtain the expression for $(\nabla_t \cdot \vec{e}_t)[\vec{e}_t \cdot \nabla_t (\ln n^2(r, \varphi))]$ for the y polarization, we change $\cos(\varphi)$ to $\sin(\varphi)$ and $\sin(\varphi)$ to $-\cos(\varphi)$ in the result of $(\nabla_t \cdot \vec{e}_t)$, then

$(\nabla_t \cdot \vec{e}_t)[\vec{e}_t \cdot \nabla_t (\ln n^2(r, \varphi))]$ for the y polarization becomes

$$\begin{aligned}
(\nabla_t \cdot \vec{e}_t)[\vec{e}_t \cdot \nabla_t (\ln n^2(r, \varphi))] &= [f'_0(r) \sin(\varphi) + e(\hat{f}'_1(r) \sin(\varphi) \cos(2\varphi) - \\
(2/r) \hat{f}_1 \cos(\varphi) \sin(2\varphi)] [f_0(r) + e \hat{f}_1(r) \cos(2\varphi)].g(r, \varphi) [\sin(\varphi) - 2e \cos(\varphi) \sin(2\varphi)] \\
&= g_y(r, \varphi)
\end{aligned}$$

Now, we have

$$(\tilde{\beta}^2 - \beta_x^2) - (\tilde{\beta}^2 - \beta_y^2) = \beta_y^2 - \beta_x^2 = (\beta_y - \beta_x) (\beta_y + \beta_x) \cong 2\beta_0 \delta\beta_{xy}$$

$$= \left(\int_S [g_x(r, \varphi) - g_y(r, \varphi)] ds \right) / \left(\int_S \psi^2(r, \varphi) ds \right) \quad (4.34)$$

In order to evaluate the integration above, first we will find simplified expressions for $g_x(r, \varphi)$ - $g_y(r, \varphi)$ and $\psi^2(r, \varphi)$. To find an expression for $[g_x(r, \varphi) - g_y(r, \varphi)]$, we substitute the functions defined previously for $g_x(r, \varphi)$, $g_y(r, \varphi)$, and $g(r, \varphi)$, and by neglecting terms of order of (e^2) we obtain the following

$$g_x(r,\varphi) - g_y(r,\varphi) = 2 \sum_{i=1}^3 ((n_{i+1} - n_i)/n_i) \delta[r - a_i (1 + e \cos(2\varphi))].$$

$$\{ f_0(a_i) f'_o(a_i) \cos(2\varphi) + e [a_i [f_0(a_i) f''_o(a_i) + (f'_o(a_i))^2] \cos^2(2\varphi)$$

$$- 2 f_0(a_i) f'_o(a_i) \sin^2(2\varphi) + [f_0(a_i) \hat{f}'_1(a_i) + f'_o(a_i) \hat{f}_1(a_i)] \cos^2(2\varphi)$$

$$+ (2/a_i) f_0(a_i) \hat{f}_1(a_i) \sin^2(2\varphi) \} + 0 (e^2)$$

and

$$\int_{\varphi=0}^{2\pi} \int_{r=0}^{\infty} [g_x(r,\varphi) - g_y(r,\varphi)] r dr d\varphi = 2\pi e \left\{ \sum_{i=1}^3 ((n_{i+1} - n_i)/n_i) Q_i \right\} + 0(e^2) = 2\pi e Q$$

where

$$Q_i = f_0(a_i) [-a_i f'_o(a_i) + a_i^2 f''_o(a_i) + 2 \hat{f}_1(a_i) + a_i \hat{f}'_1(a_i)] + a_i f'_o [a_i f'_o(a_i) + \hat{f}_1(a_i)]$$

The denominator for the $2\beta_o \delta\beta_{xy}$ expression is

$$d = \left(\int_s \psi^2(r,\varphi) ds \right) = 2\pi \int_0^{\infty} f_0^2(r) r dr$$

finally the birefringence is

$$\delta\beta_{xy} = (1/2\beta_o) (eQ)/(d) \tag{4.35}$$

and the normalized birefringence is

$$\delta\beta_{xy}/e = (1/2\beta_0) (Q)/(d) \quad (4.36)$$

where

$$\begin{aligned} d &= \int_0^{a_2} f_0^2(r) r dr + \int_{a_3}^{\infty} B_4^2 K_0^2(u_4 r) r dr \\ &= \int_0^{a_2} f_0^2(r) r dr + (1/2) \alpha_3^2 B_4^2 [K_0'^2(U_4) - K_0^2(U_4)] \end{aligned}$$

Since λ and α_i ; $i = 1, 2,$ and 3 are measured in μm , the unit for $(\delta\beta_{xy}/e)$ is μm^{-1} .

4.2.2.4 Effective Area (Aeff) and Mode-Field Diameter (MFD)

The expression for the effective area (Aeff) is given by [113]

$$A_{\text{eff}} = \frac{\left[\int_0^{2\pi} \int_0^{\infty} |\psi(r, \phi)|^2 r dr d\phi \right]^2}{\int_0^{2\pi} \int_0^{\infty} |\psi(r, \phi)|^4 r dr d\phi} \quad (4.37)$$

and for the fundamental mode reduces to

$$A_{\text{eff}} = (2\pi) \frac{\left[\int_0^{\infty} |\psi(r)|^2 r dr \right]^2}{\int_0^{\infty} |\psi(r)|^4 r dr} \quad (4.38)$$

The expression used to calculate the mode-field diameter (MFD) is based on the Petermann II definition [114]

$$\text{MFD} = \sqrt{(8) \frac{\int_0^{\infty} |\psi(r)|^2 r dr}{\int_0^{\infty} |d\psi(r) / dr|^2 r dr}} \quad (4.39)$$

4.3 DESIGN OF ZERO POLARIZATION-MODE DISPERSION FIBER

In order to achieve zero PMD as a principal goal, several refractive-index profiles were examined. The design of zero PMD fiber was carried out by varying the material compositions and adjusting the dimensions of various layers. For all tested profiles, the requirements of having small chromatic dispersion, single-mode operation, and practical dimensions were taken into consideration. The results obtained for the examined profiles indicate that a multiple-clad geometry with depressed core, shown in Figure 4.2, is suitable for the design of zero PMD fiber. The basis of choosing this profile is not solely to meet the previously stated requirements, but also considering other factors that play an important role in present communication systems as well. In particular, among such factors are effective area and mode-field diameter.

The fiber parameters and material compositions for an example design are summarized in Table 4.1. The proposed dispersion-shifted fiber offers several improvements in fiber communications links as discussed next.

In order to achieve zero PMD at the operating wavelength ($\lambda = 1.55 \mu\text{m}$), the two x and y polarizations of the fundamental LP_{01} mode must have the same group velocity. The group velocity is defined as $v_g = d\omega/d\beta = c(dk_o/d\beta)$, where $k_o = \omega/c = 2\pi/\lambda$ is the free

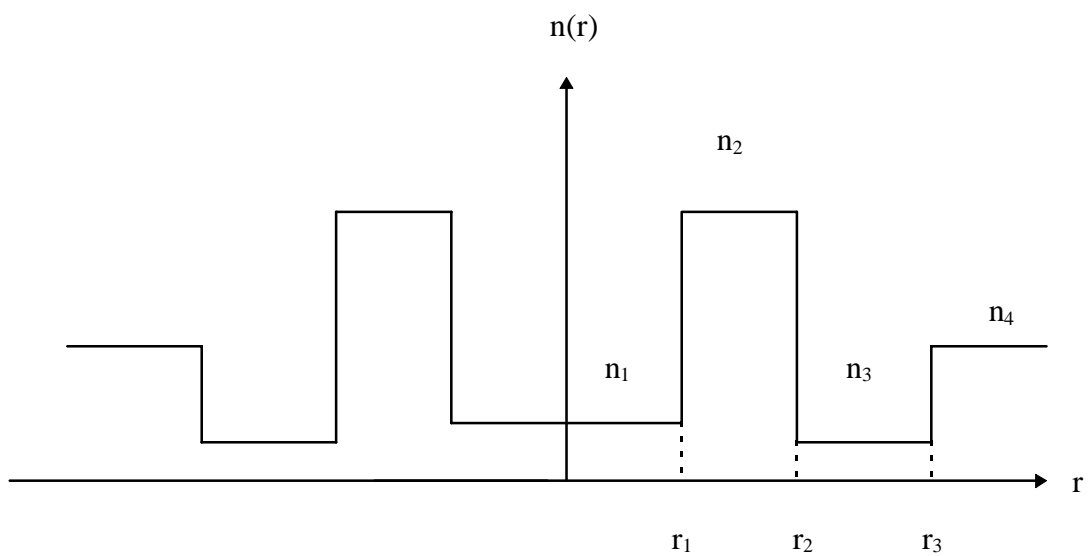


Figure 4.2 Refractive-index profile used for the design of zero PMD fiber.

Table 4.1 Materials and Radii of Designed Dispersion-Shifted Fiber For Zero PMD.

	Core	Clad1	Clad2	Clad3
Material	M5	M2	M9	M3
Radius	2.9 μm	4.2 μm	5 μm	∞

space wave number, c is the speed of light in free space, and β is the propagation constant. The two polarizations will have the same group velocity when the $d(\beta + \delta\beta_x)/dV = d(\beta + \delta\beta_y)/dV$. In other words, when $(\beta_x - \beta_y) = \delta\beta_{xy} = (\delta\beta_x - \delta\beta_y)$ is maximum/minimum, the two polarizations have the same group velocity and therefore the PMD is zero at the corresponding wavelength.

A normalized birefringence parameter is defined as $\delta\beta_{xy}/e$. Figure 4.3 illustrates the normalized birefringence versus wavelength for the fiber specified in Table 4.1. This plot shows that the minimum of birefringence occurs at 1.55 μm . The significance of this result is zero PMD in the single-mode operation, whereas in typical single-mode fiber this occurs outside the single-mode operation. The normalized propagation constant b , defined in (4.6), is calculated and plotted versus wavelength for the fundamental LP_{01} mode in Figure 4.4. The cutoff wavelength of the next higher order mode, LP_{11} , is found to be 1.45 μm , which ensures a single-mode operation at 1.55 μm .

Figure 4.5 shows variations of chromatic dispersion versus wavelength. The dispersion calculated at 1.55 μm is 0.65 ps/nm.km, and the dispersion slope at this wavelength is 0.055 ps/nm².km.

Two other important parameters are the effective area and mode-field diameter. The variations of the effective area and the mode-field diameter as a function of wavelength have been calculated and shown in Figures 4.6 and 4.7, respectively. At 1.55 μm , the effective area is 122.5 μm^2 and the mode-field diameter is 10.5 μm . The fiber design offers a larger effective area compared to those of conventional and low-nonlinearity

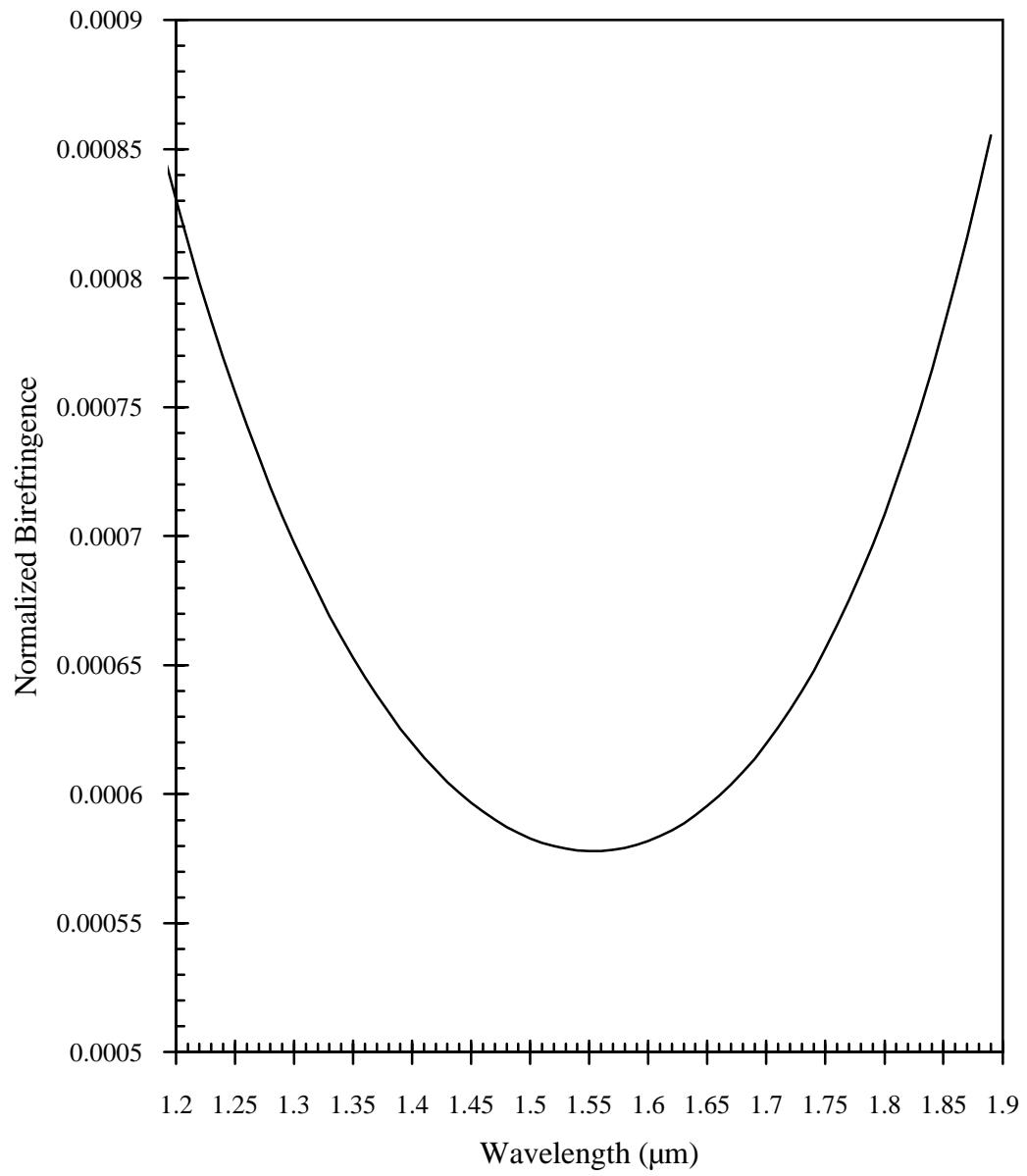


Figure 4.3 Normalized birefringence ($\delta\beta_{xy}/e$) versus wavelength of fundamental LP_{01} mode.

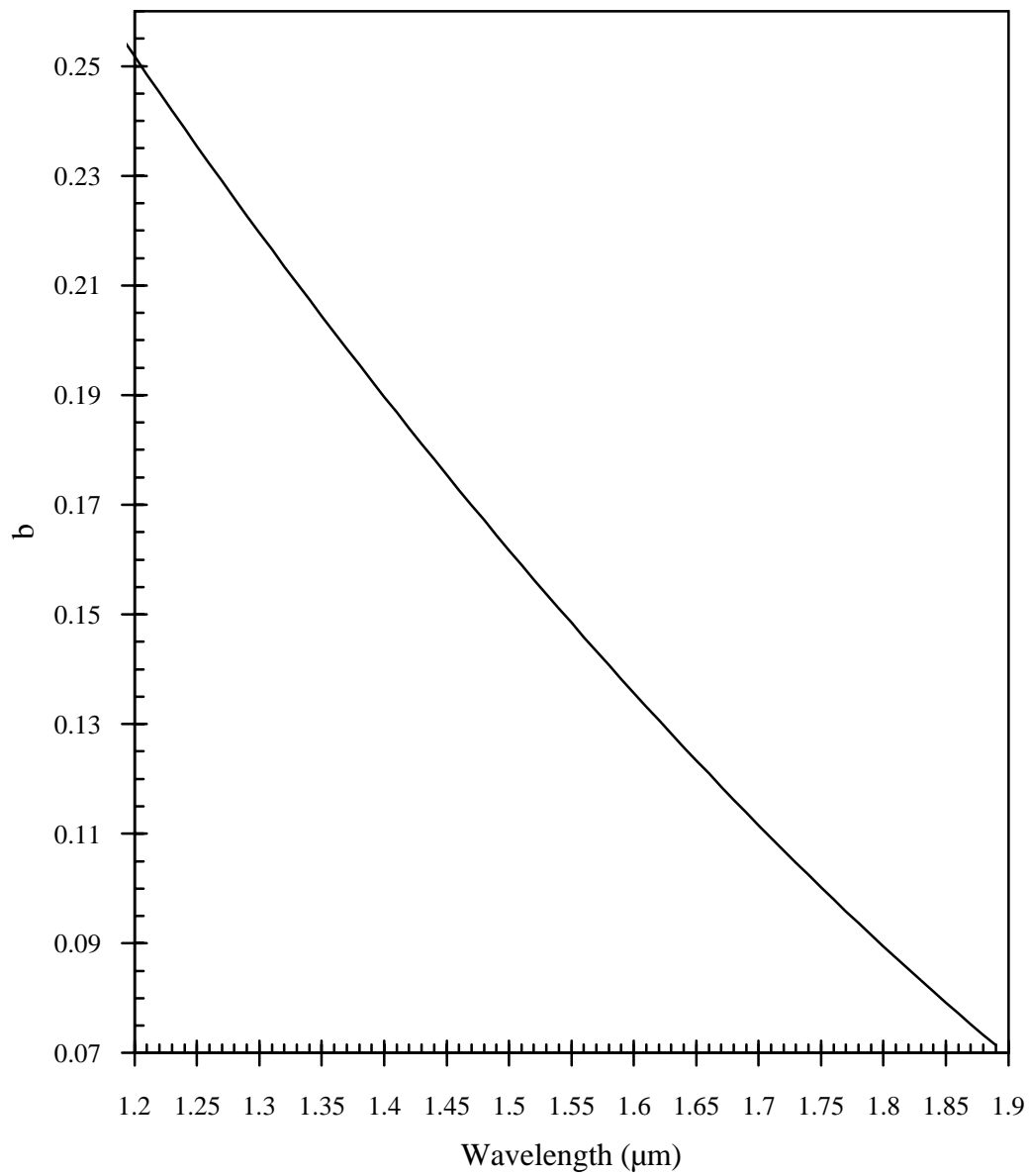


Figure 4.4 Normalized propagation constant b versus wavelength of fundamental LP_{01} mode.

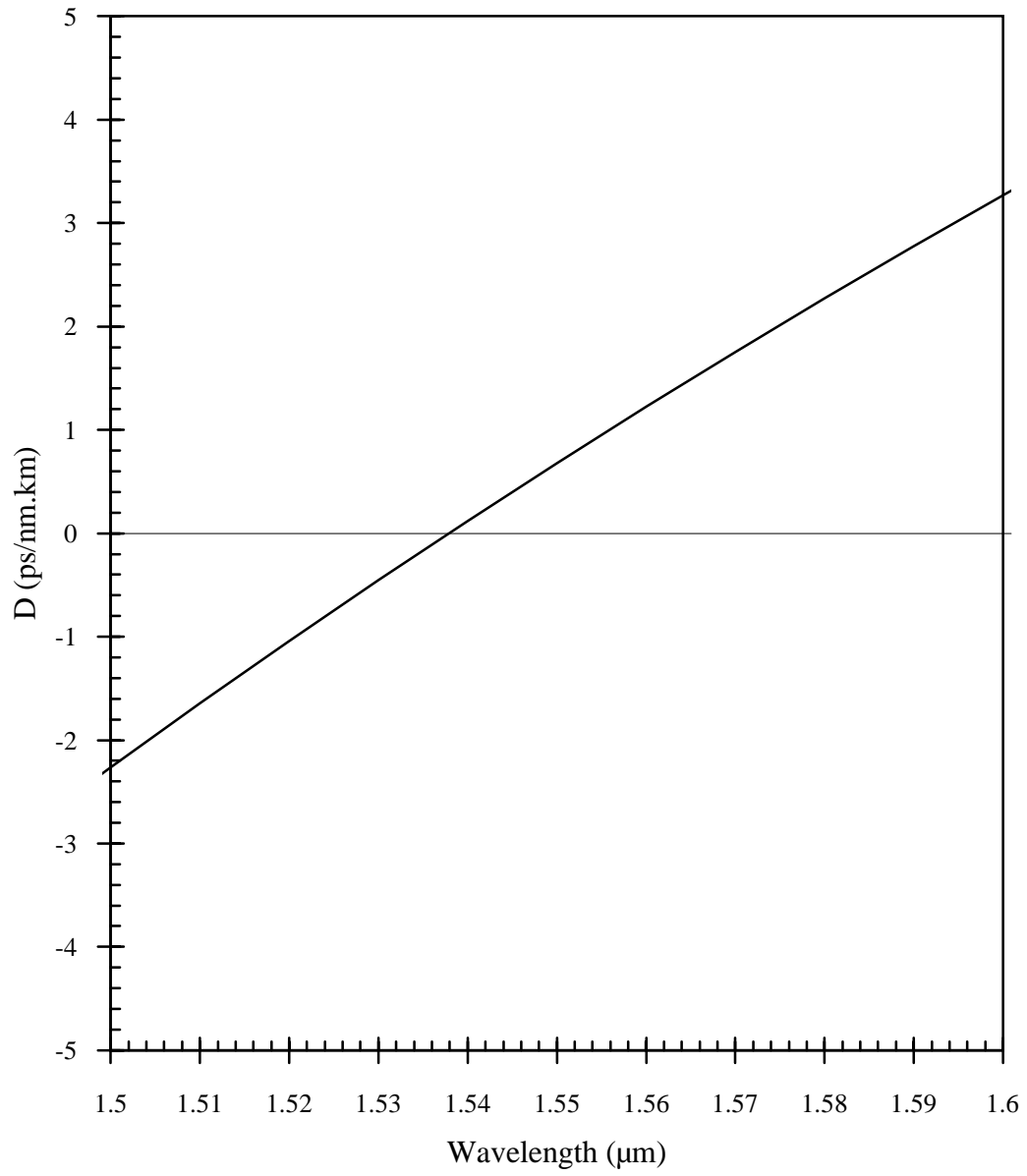


Figure 4.5 Dispersion versus wavelength of fundamental LP₀₁ mode.

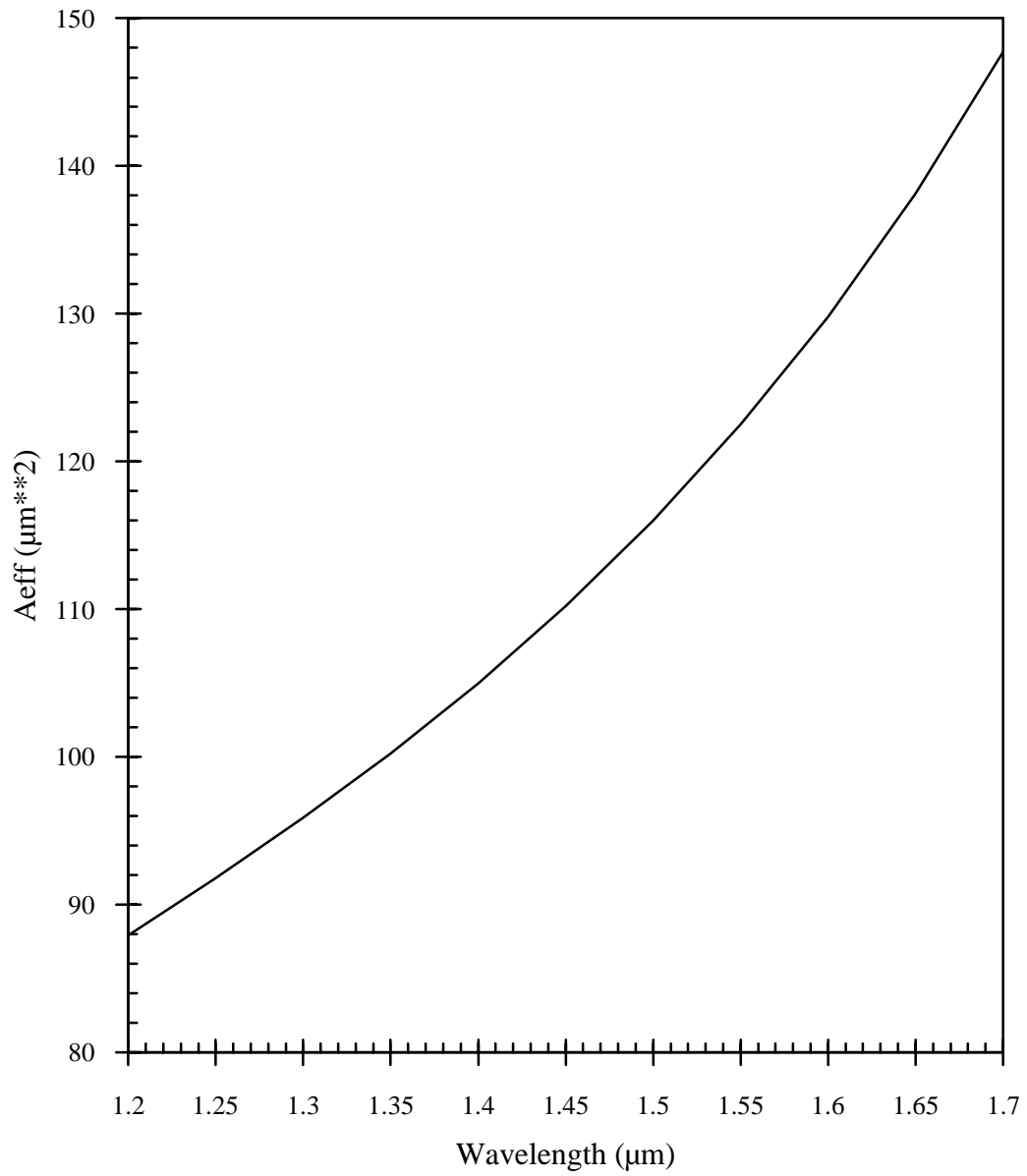


Figure 4.6 Effective area versus wavelength of fundamental LP_{01} mode.

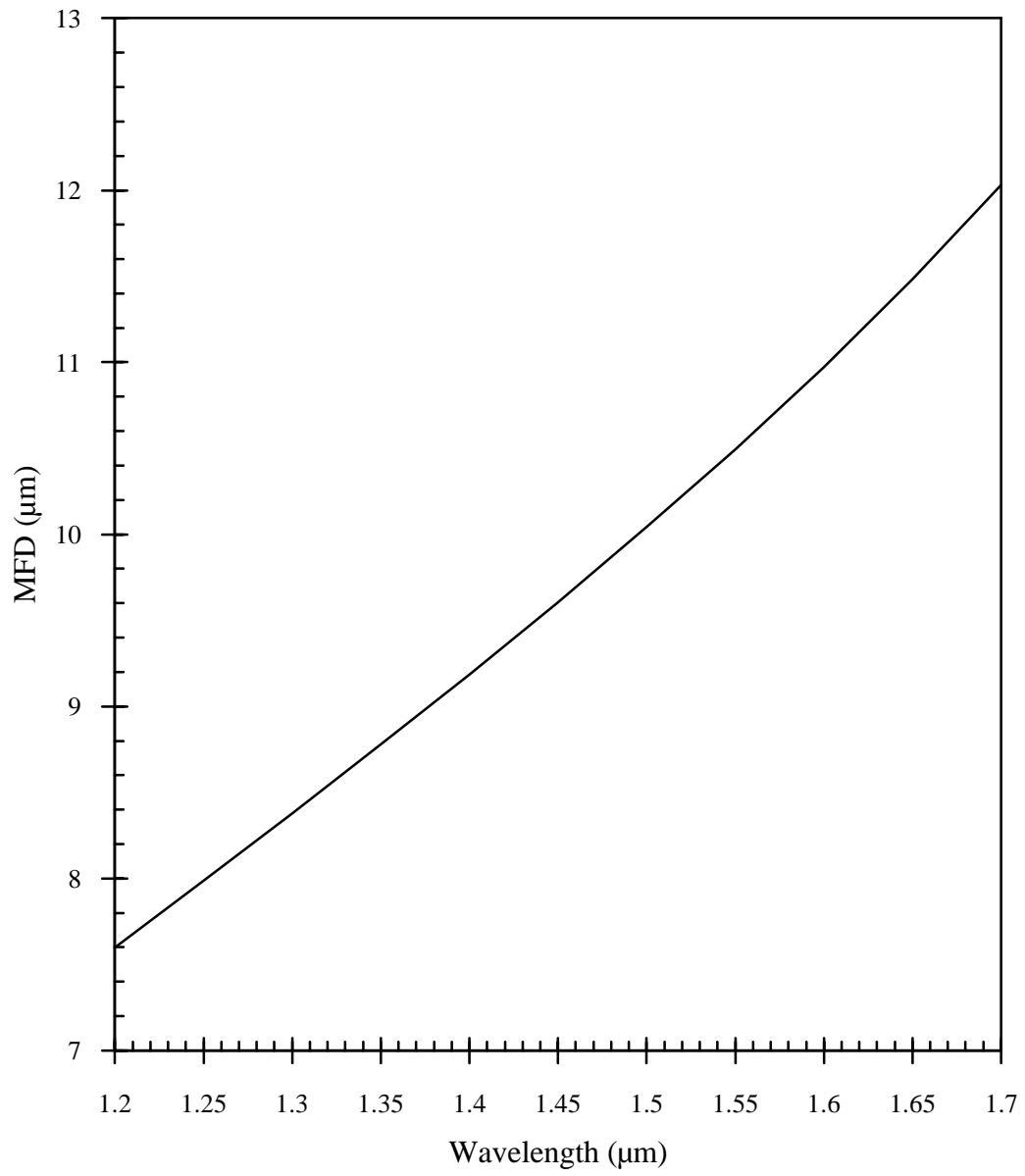


Figure 4.7 Mode-Field Diameter versus wavelength of fundamental LP₀₁ mode.

Table 4.2 Transmission Properties of Zero PMD Dispersion-Shifted Fiber At $\lambda = 1.55 \mu\text{m}$.

Dispersion	Dispersion Slope	Mode-Field Diameter	Effective Area	Cutoff Wavelength of LP₁₁ Mode
0.65 ps/nm.km	0.055 ps/nm ² .km	10.5 μm	122.5 μm^2	1.42 μm

dispersion-shifted fibers [19] whose range is between $50 \mu\text{m}^2$ to $90 \mu\text{m}^2$. The mode-field diameter value is about the same as the maximum value accepted for minimum losses in fiber for high capacity transmission applications. Also, bending loss is calculated and plotted versus bending radius in Figure 4.8.

The transmission characteristics of the designed fiber are tabulated in Table 4.2 at an operating wavelength of $1.55 \mu\text{m}$.

4.4 TOLERANCE ANALYSIS

Tolerance analysis due to variation in the radii of the designed fiber's layers is conducted in order to simulate the effects of such variations which may occur in manufacturing processes. The effects on the normalized birefringence and chromatic dispersion versus wavelength will be shown numerically due to variation in one of the fiber's layers radius at a time.

4.4.1 Polarization Mode Dispersion

The variations in the radii of the layers are taken as $\pm 1\%$ and $\pm 2\%$. Starting with the normalized birefringence, Figures 4.9, 4.10, and 4.11 display the behavior of normalized birefringence versus wavelength as a result of radii variations of the first, second, and third layer, respectively. The fourth layer is considered to extend to infinity in the radial direction, and therefore no radius variation is considered. Examining these three figures

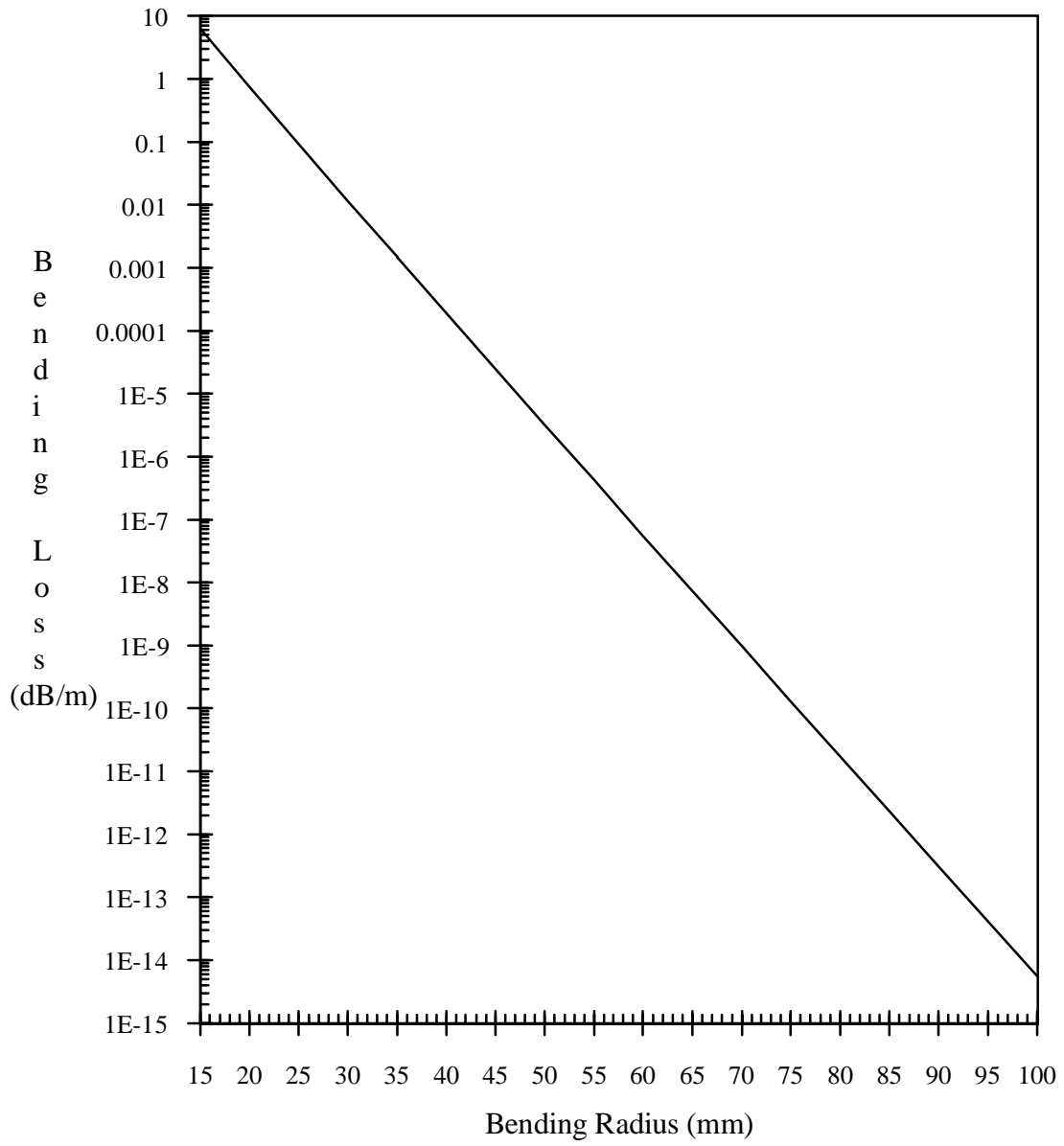


Figure 4.8 Bending loss versus bending radius of fundamental LP₀₁ mode.

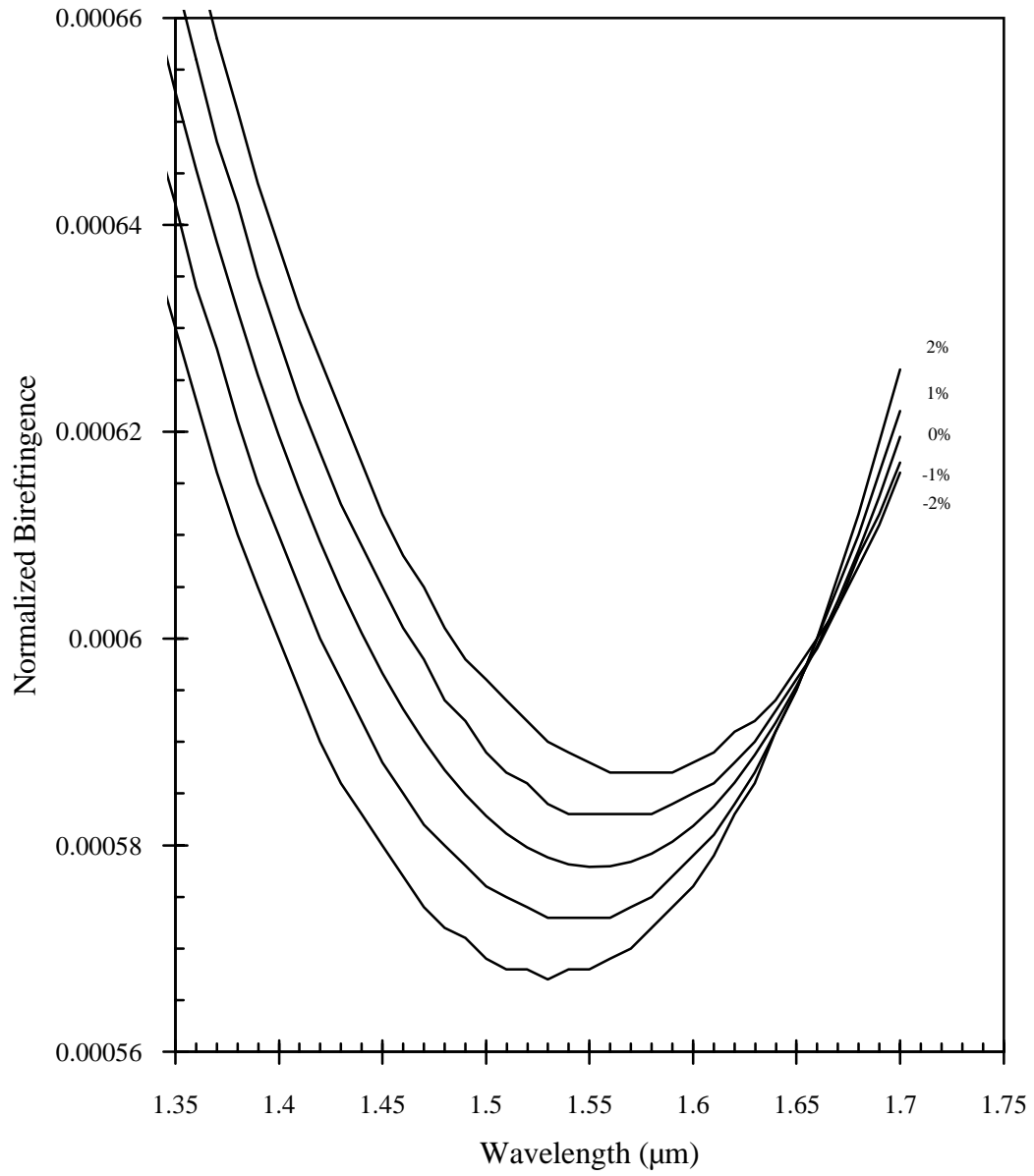


Figure 4.9 Variations of normalized birefringence ($\delta\beta_{xy}/e$) versus wavelength of fundamental LP_{01} mode for radius α_1 variations of $\pm 1\%$ and $\pm 2\%$.

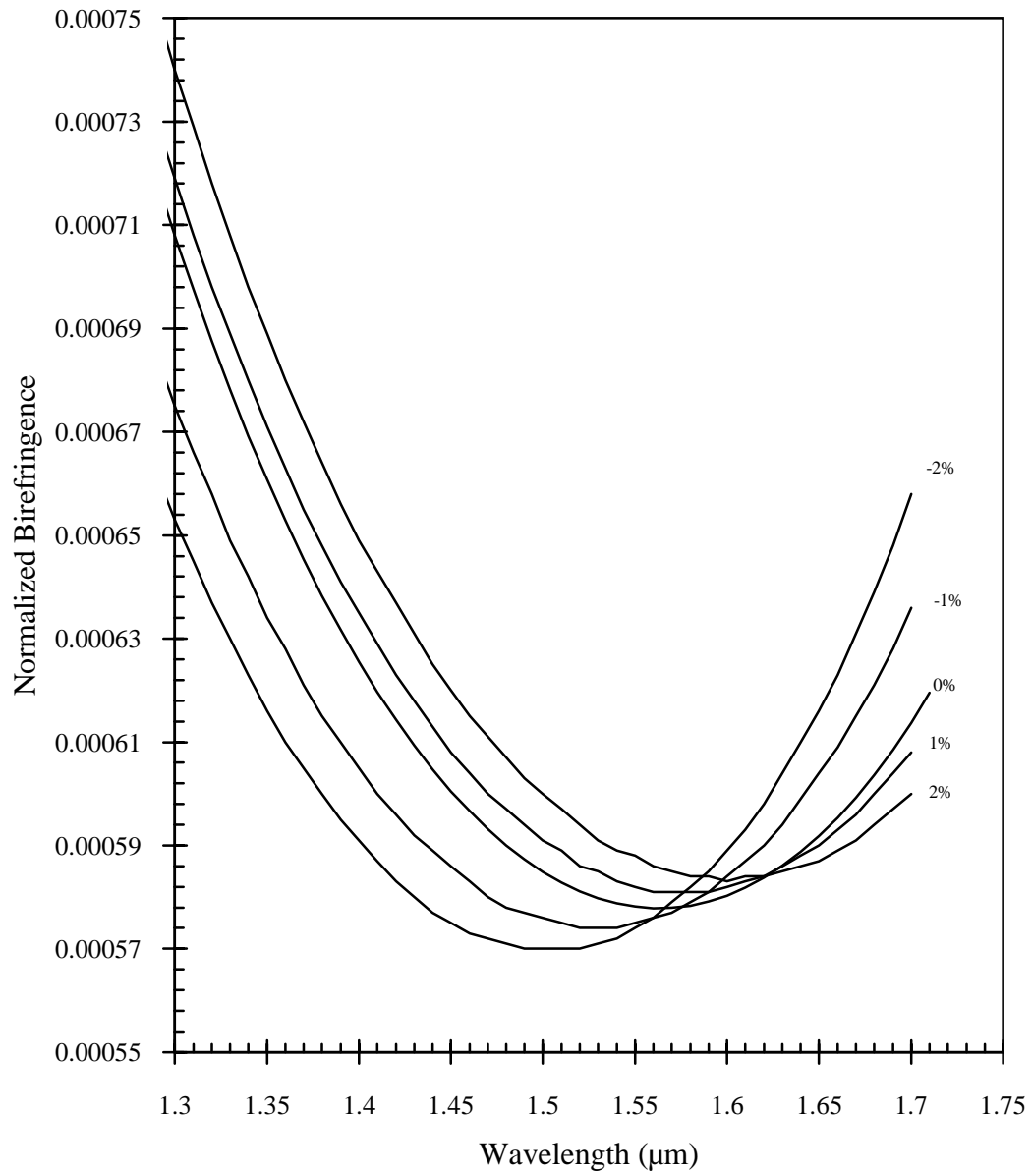


Figure 4.10 Variations of normalized birefringence ($\delta\beta_{xy}/e$) versus wavelength of fundamental LP_{01} mode for radius α_2 variations of $\pm 1\%$ and $\pm 2\%$.

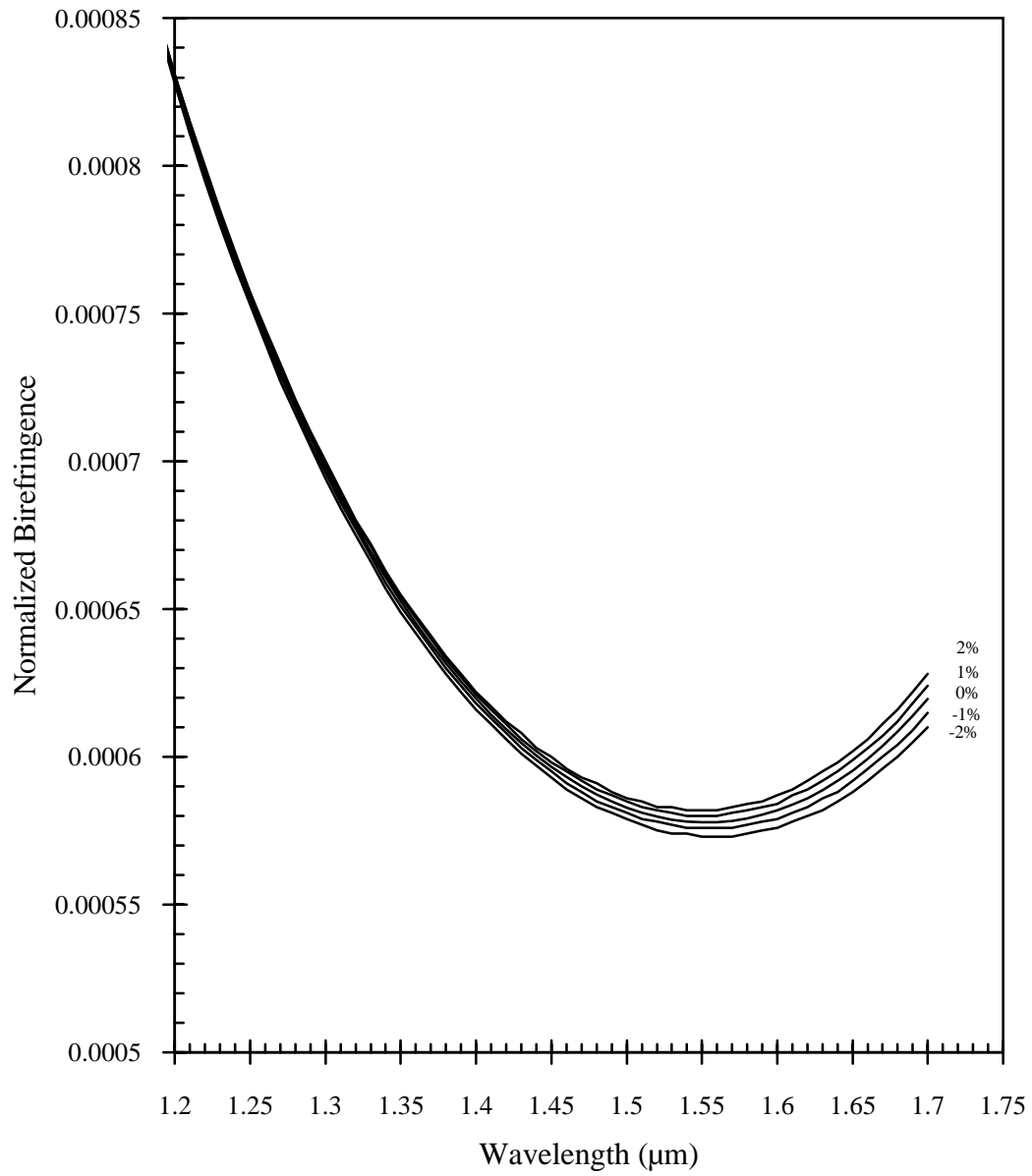


Figure 4.11 Variations of normalized birefringence ($\delta\beta_{xy}/e$) versus wavelength of fundamental LP_{01} mode for radius α_3 variations of $\pm 1\%$ and $\pm 2\%$.

Table 4.3 The Wavelength At Which Normalized Birefringence Peak Occurs As The Radii α_i ($i = 1, 2,$ and 3) Of The Fiber Changes.

Percent Variations of R_{ii} α_i	λ of Birefringence Peak Due To Radius α_1 Changes	λ of Birefringence Peak Due To Radius α_2 Changes	λ of Birefringence Peak Due To Radius α_3 Changes
-2%	1.57 μm	1.5 μm	1.56 μm
-1%	1.56 μm	1.53 μm	1.56 μm
0%	1.55 μm	1.55 μm	1.55 μm
1%	1.54 μm	1.58 μm	1.55 μm
2%	1.53 μm	1.6 μm	1.55 μm

shows that the parameter that has the most effect is the radius of the second layer, α_2 . The numerical results show that the peak of the normalized birefringence has shifted either to upper or lower wavelength compared to the original design. The wavelengths at which the peak occurs due to α_2 variations are shown in Table 4.3. The variations of radius α_3 has the least effect on the normalized birefringence where the peak stayed at about 1.55 μm , as shown in Table 4.3. The effect of varying radius α_1 as shown in Table 4.3 and Figure 4.9 is about moderate and not much significant on the normalized birefringence peak with the specified percent variations.

4.4.2 Chromatic Dispersion

The next tolerance analysis is performed on the chromatic dispersion by varying the radii of the fiber's layers one at a time the same way that was carried out for the normalized birefringence previously. The percent variations of the radii are also considered to be $\pm 1\%$ and $\pm 2\%$. Figures 4.12, 4.13, and 4.14 show the variations of the chromatic dispersion versus wavelength due to variations in the fiber's radii. The numerical values of

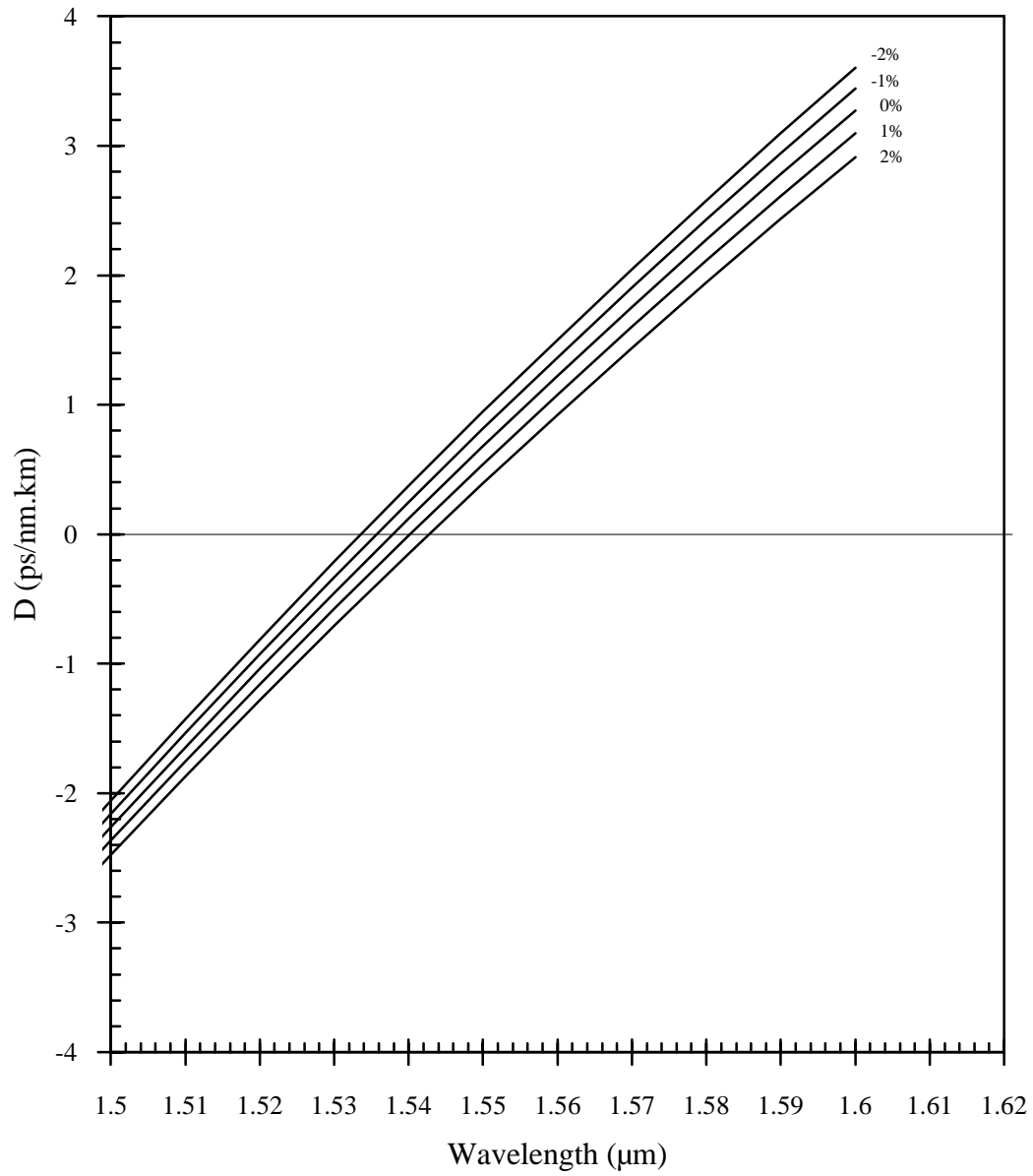


Figure 4.12 Variations of chromatic dispersion versus wavelength of fundamental LP₀₁ mode for radius a_1 variations of $\pm 1\%$ and $\pm 2\%$.

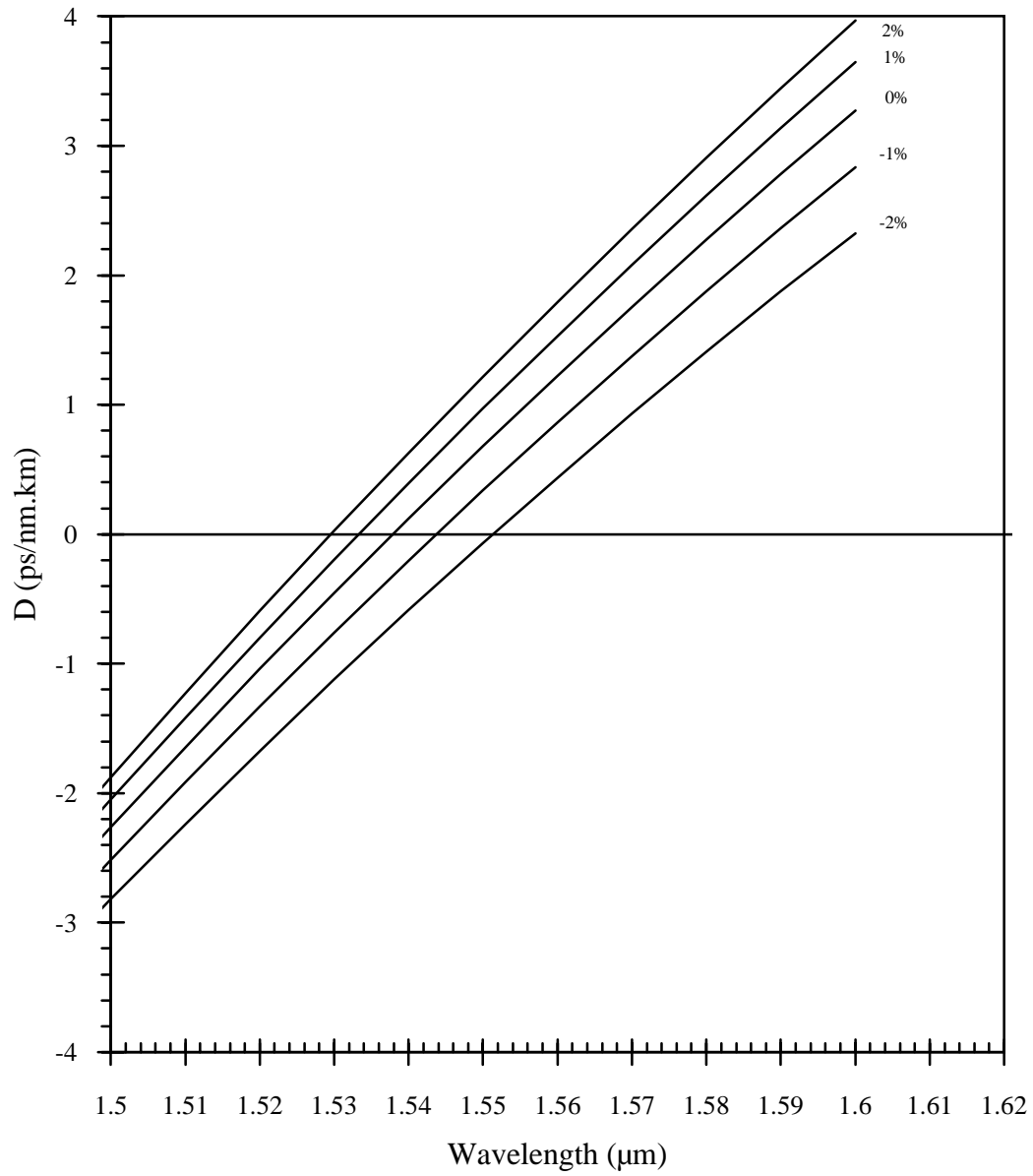


Figure 4.13 Variations of chromatic dispersion versus wavelength of fundamental LP_{01} mode for radius a_2 variations of $\pm 1\%$ and $\pm 2\%$.

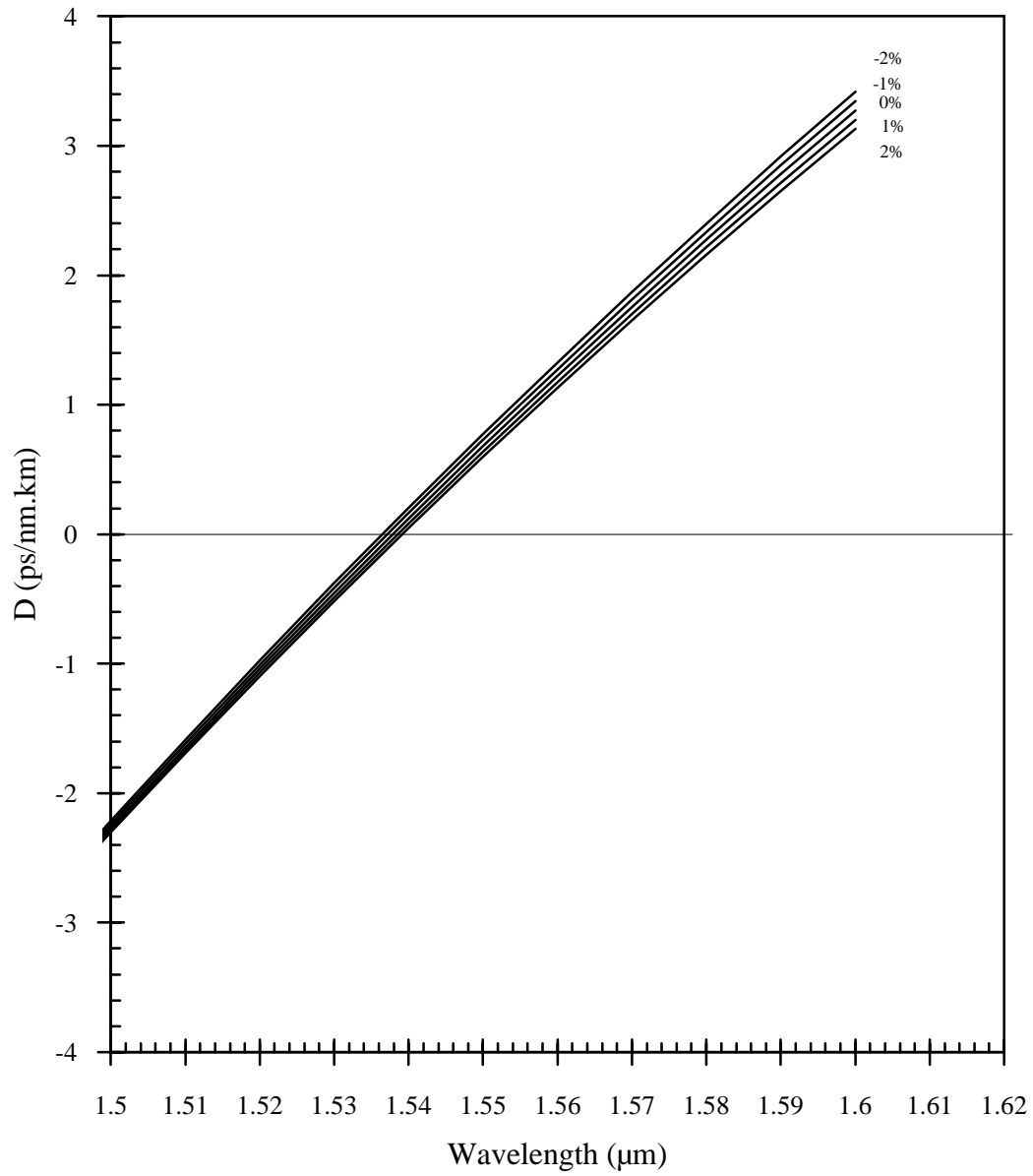


Figure 4.14 Variations of chromatic dispersion versus wavelength of fundamental LP₀₁ mode for radius a_3 variations of $\pm 1\%$ and $\pm 2\%$.

Table 4.4 Chromatic Dispersion Values in ps/(nm.km) At $\lambda = 1.55 \mu\text{m}$ As The Radius α_i ($i = 1, 2,$ and 3) Of The Fiber Changes.

Percent Variations of Rdi α_i	Dispersion Due To Radius α_1 Changes	Dispersion Due To Radius α_2 Changes	Dispersion Due To Radius α_3 Changes
-2%	0.944	-0.067	0.773
-1%	0.814	0.337	0.725
0%	0.679	0.679	0.679
1%	0.54	0.97	0.64
2%	0.393	1.22	0.595

the dispersion are shown in Table 4.4 indicating, in the same manner as in the previous tolerance analysis done for the normalized birefringence, that the radius of the second layer α_2 is the most critical parameter compared to the other radii α_1 and α_3 . The radius of the first layer α_1 has some effect on the dispersion but not drastically; while the radius of the third layer α_3 has the least and almost minor effect. Taking these calculations one step further, the wavelengths at which zero or close to zero dispersion (less than 0.09 ps/(nm.km)) occur are determined and listed in Table 4.5 for the specified percent variations of the fiber's radii. However, sometimes positive or negative dispersion are needed in fiber design for communications links to reduce signal distortions due to nonlinearity in fiber.

4.4.3 Effective Area and Mode-Field Diameter

The tolerance analysis has also been carried out for the effective area and mode-field diameter of the designed fiber. In the same manner as has been done for the chromatic and polarization-mode dispersion, the radii of the fiber layers have been varied and the

Table 4.5 The Wavelength At Which Chromatic Dispersion Is Zero Or Close To Zero (less than 0.09 ps/(nm.km)) As The Radius α_i ($i = 1, 2,$ and 3) Of The Fiber Changes.

Percent Variations of R_{dii} α_i	λ of Zero Dispersion Due To Radius α_1 Changes	λ of Zero Dispersion Due To Radius α_2 Changes	λ of Zero Dispersion Due To Radius α_3 Changes
-2%	1.535 μm	1.55 μm	1.538 μm
-1%	1.535 μm	1.545 μm	1.538 μm
0%	1.535 μm	1.535 μm	1.535 μm
1%	1.545 μm	1.535 μm	1.54 μm
2%	1.545 μm	1.53 μm	1.54 μm

corresponding effective area and mode-field diameter values are evaluated. Figures 4.15, 4.16, and 4.17 show the effective area versus wavelength due to the radii variations α_1 , α_2 , and α_3 , respectively. The values of the effective area at $\lambda = 1.55 \mu\text{m}$ are determined and shown in Table 4.6. The percent variations of the fiber's radii considered in this analysis have not affected the effective area significantly, especially at $\lambda = 1.55 \mu\text{m}$. The values obtained for the effective area at $\lambda = 1.55 \mu\text{m}$ range between $117 \mu\text{m}^2$ and $128 \mu\text{m}^2$ for all the radii percent variations. The worst case of these variations is due to -2% change in α_1 in which the value of the effective area is $117.65 \mu\text{m}^2$. This value is still not significantly different from the original design's effective area value, which is $122.5 \mu\text{m}^2$. Also, it is clear from Table 4.6 and Figure 4.17 that the radius percent change of the third layer has almost no effect on the effective area, as has been demonstrated before for the other fiber transmission parameters. Even though the tolerance analysis performed on effective area due to the fiber's radii did not affect the value of the effective area significantly, generally

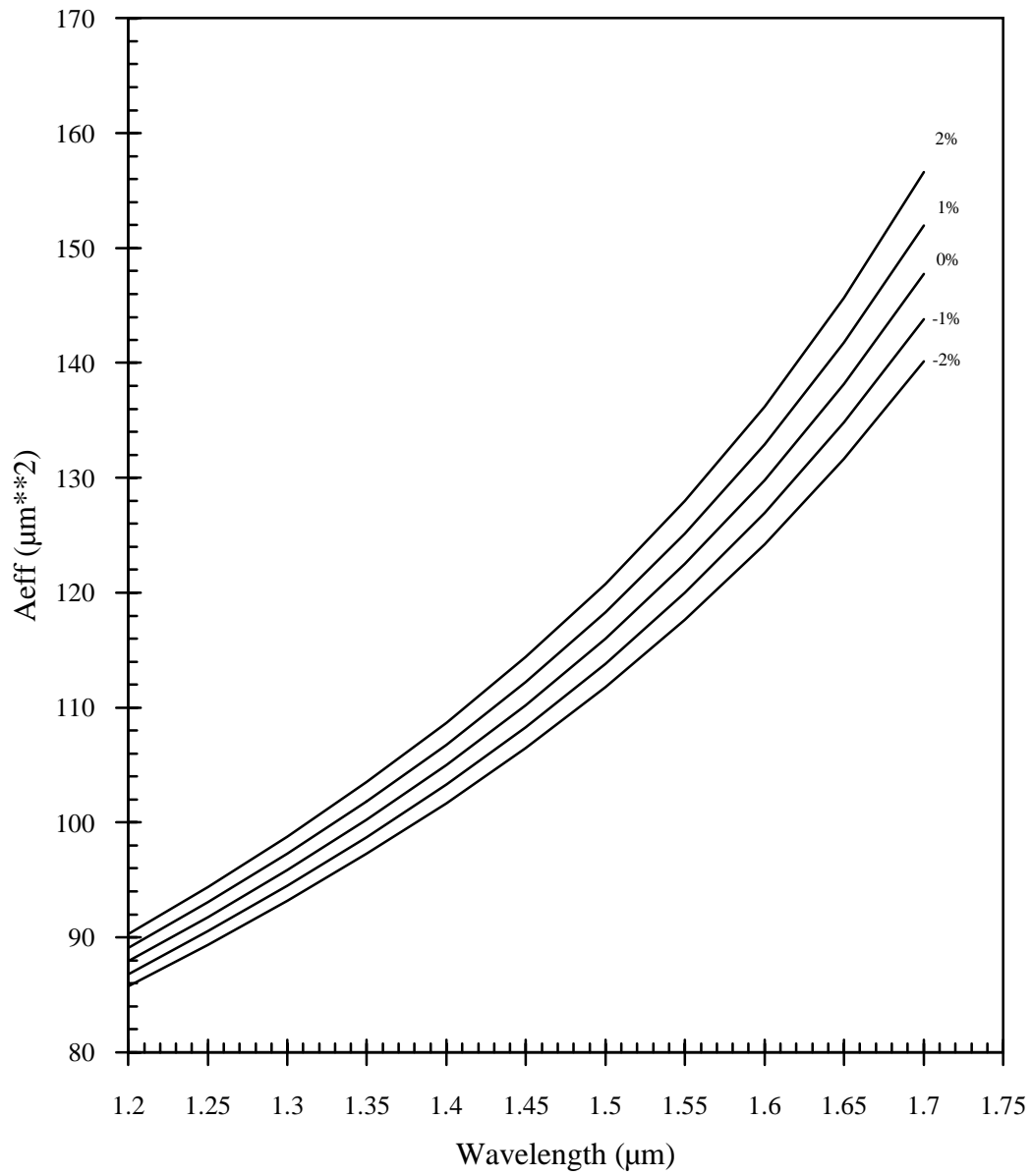


Figure 4.15 Variations of effective area versus wavelength of fundamental LP_{01} mode for radius a_1 variations of $\pm 1\%$ and $\pm 2\%$.

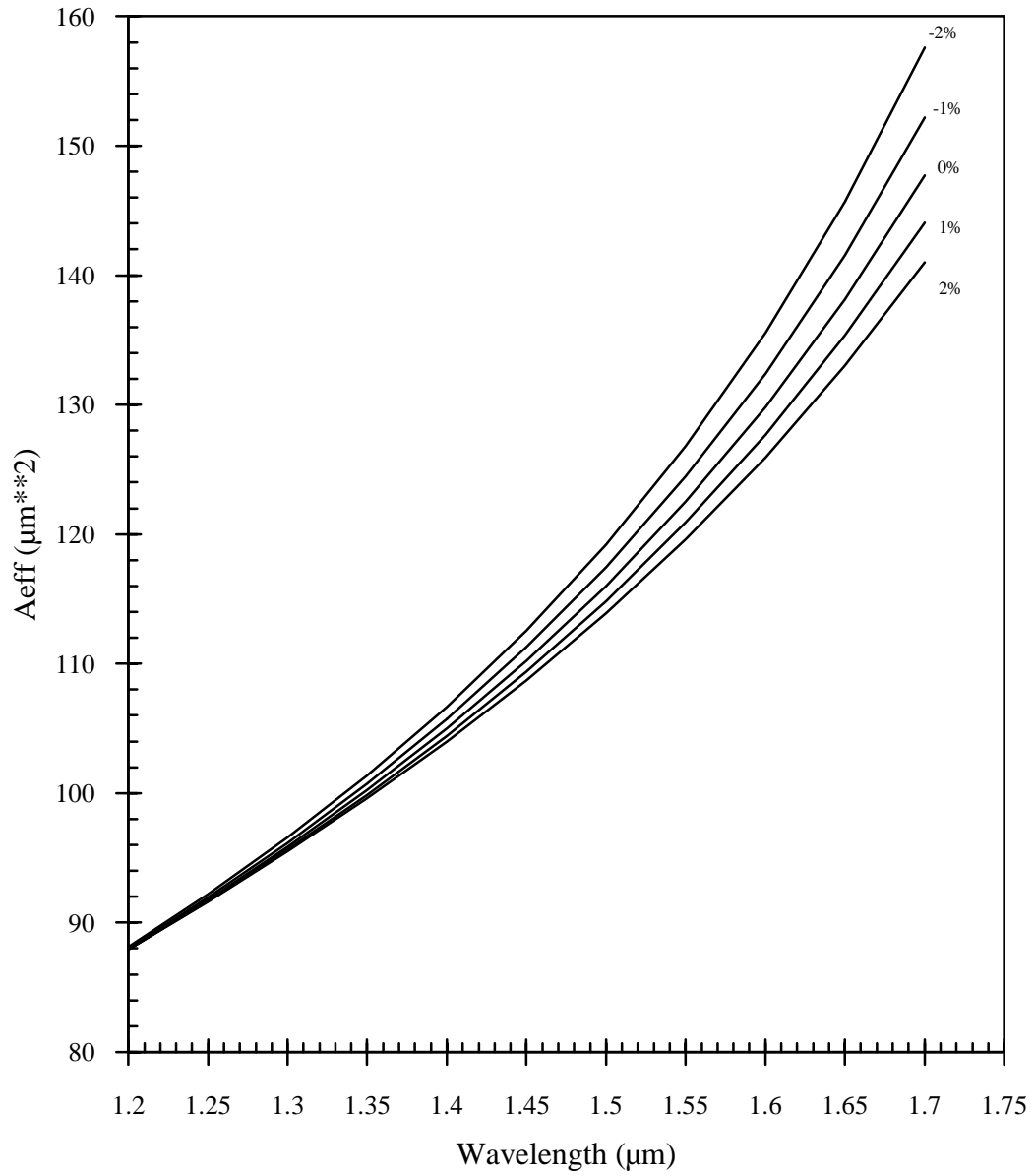


Figure 4.16 Variations of effective area versus wavelength of fundamental LP_{01} mode for radius a_2 variations of $\pm 1\%$ and $\pm 2\%$.

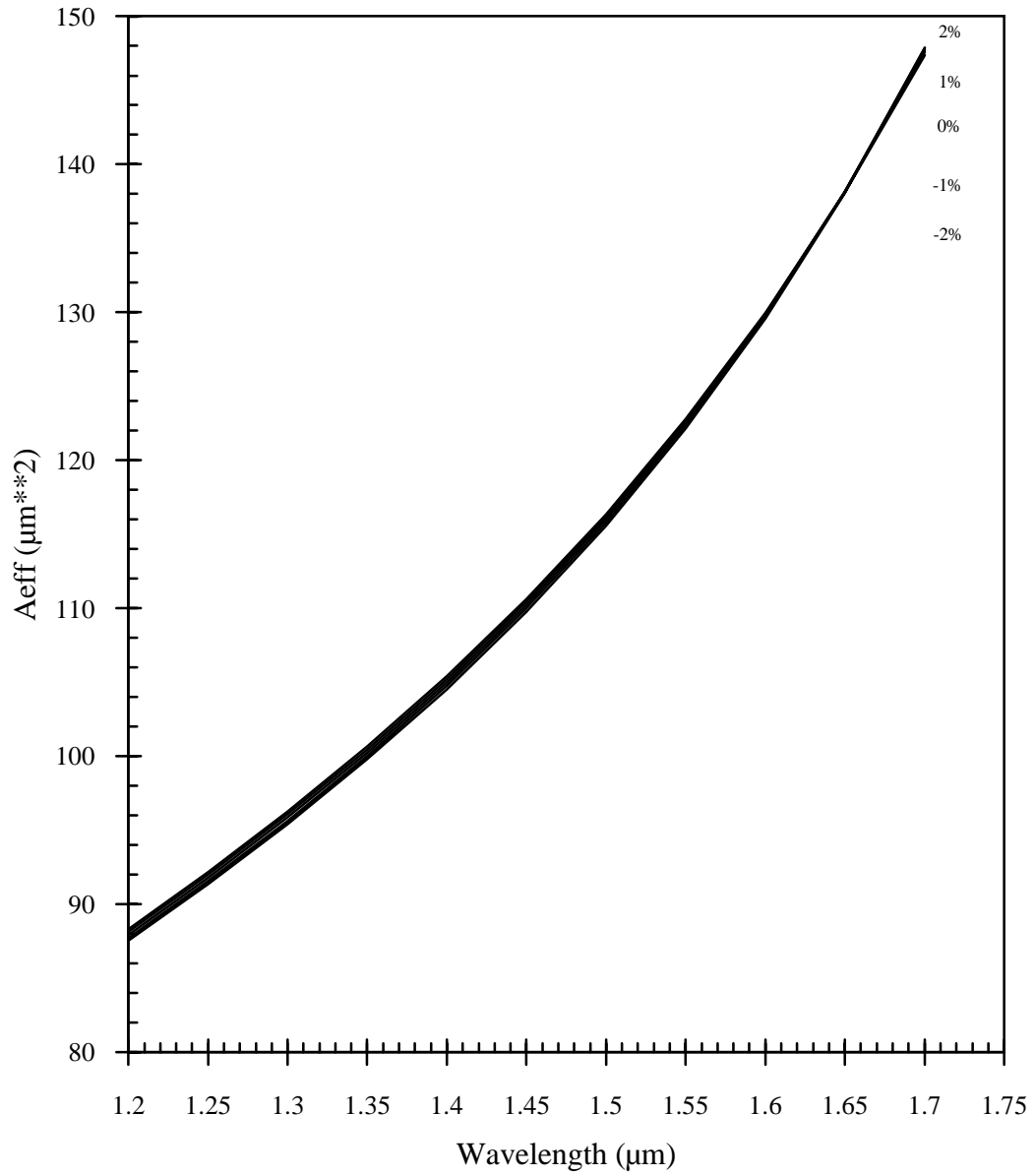


Figure 4.17 Variations of effective area versus wavelength of fundamental LP_{01} mode for radius a_3 variations of $\pm 1\%$ and $\pm 2\%$.

Table 4.6 Effective Area Values in μm^2 At $\lambda = 1.55 \mu\text{m}$ As The Radius α_i ($i = 1, 2,$ and 3) Of The Fiber Changes.

Percent Variations of Rdi α_i	Effective Area Due To Radius α_1 Changes	Effective Area Due To Radius α_2 Changes	Effective Area Due To Radius α_3 Changes
-2%	117.65	126.8	122.76
-1%	120	124.44	122.64
0%	<u>122.5</u>	<u>122.5</u>	<u>122.5</u>
1%	125	120.9	122.33
2%	128	119.6	122.14

the first layer radius has the most influence in decreasing the effective area and the second layer radius comes next.

The tolerance analysis for the mode-field diameter due to variations of the fiber's radii is performed similarly and plotted versus wavelength in Figures 4.18, 4.19, and 4.20. The mode-field diameter plots in the three figures are very close in values to each others. The original fiber design has a value of $10.5 \mu\text{m}$ for the mode-field diameter, and with the radii variations considered in this analysis the maximum value of the mode-field diameter is $10.78 \mu\text{m}$ due to -2% variation of the radius α_2 . The values obtained for the mode-field diameter at $\lambda = 1.55 \mu\text{m}$ are shown in Table 4.7. This analysis shows that the mode-field diameter is more sensitive to the radius of the second layer of the fiber than the others. This can be explained by the fact that the field is mainly confined to the second layer of the fiber, where the first layer is depressed core whose refractive index is lower than that of the second cladding.

As in all other transmission parameters results discussed previously, the third layer radius variations has negligible effect on the mode-field diameter.

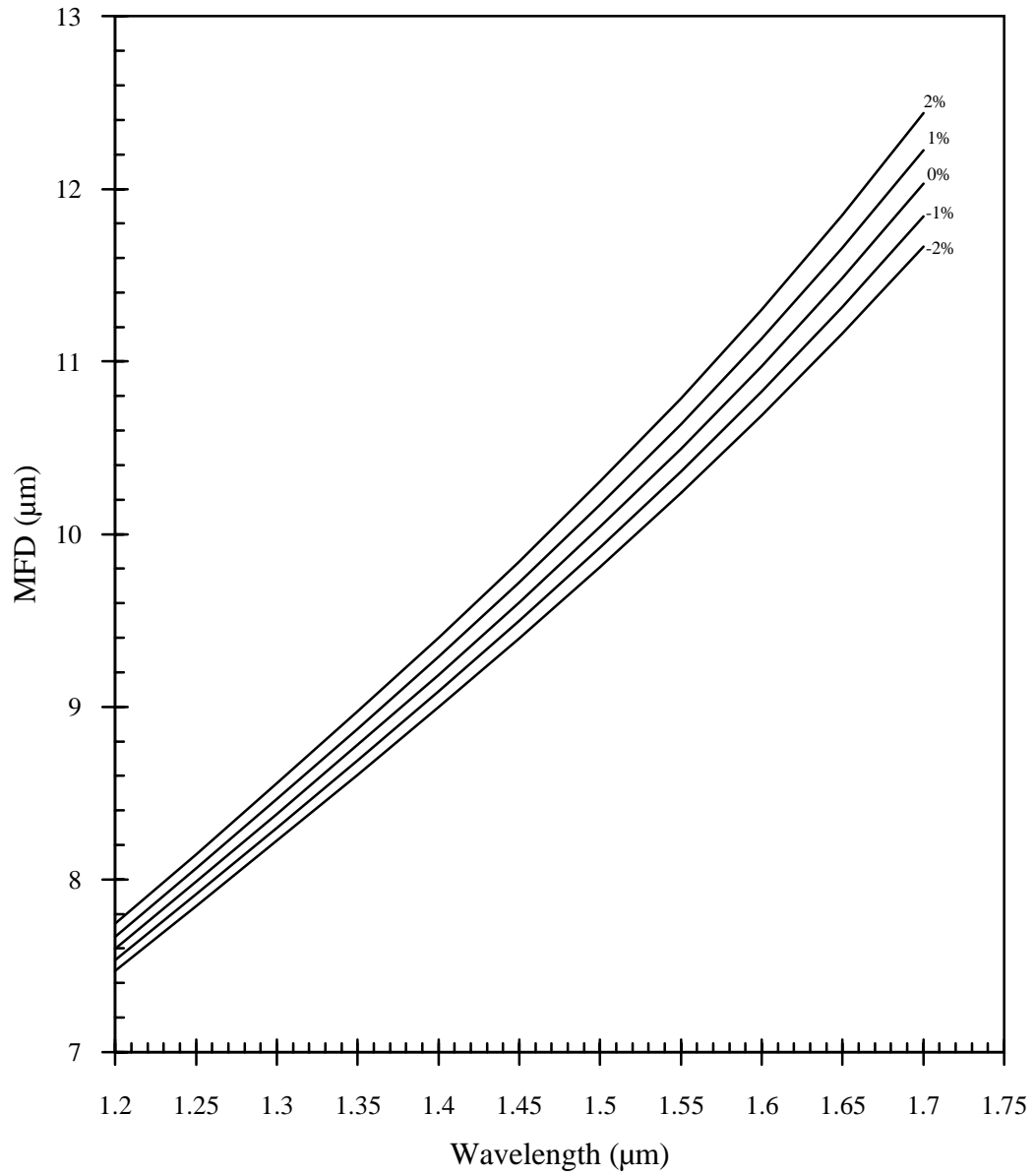


Figure 4.18 Variations of mode-field diameter versus wavelength of fundamental LP_{01} mode for radius a_1 variations of $\pm 1\%$ and $\pm 2\%$.

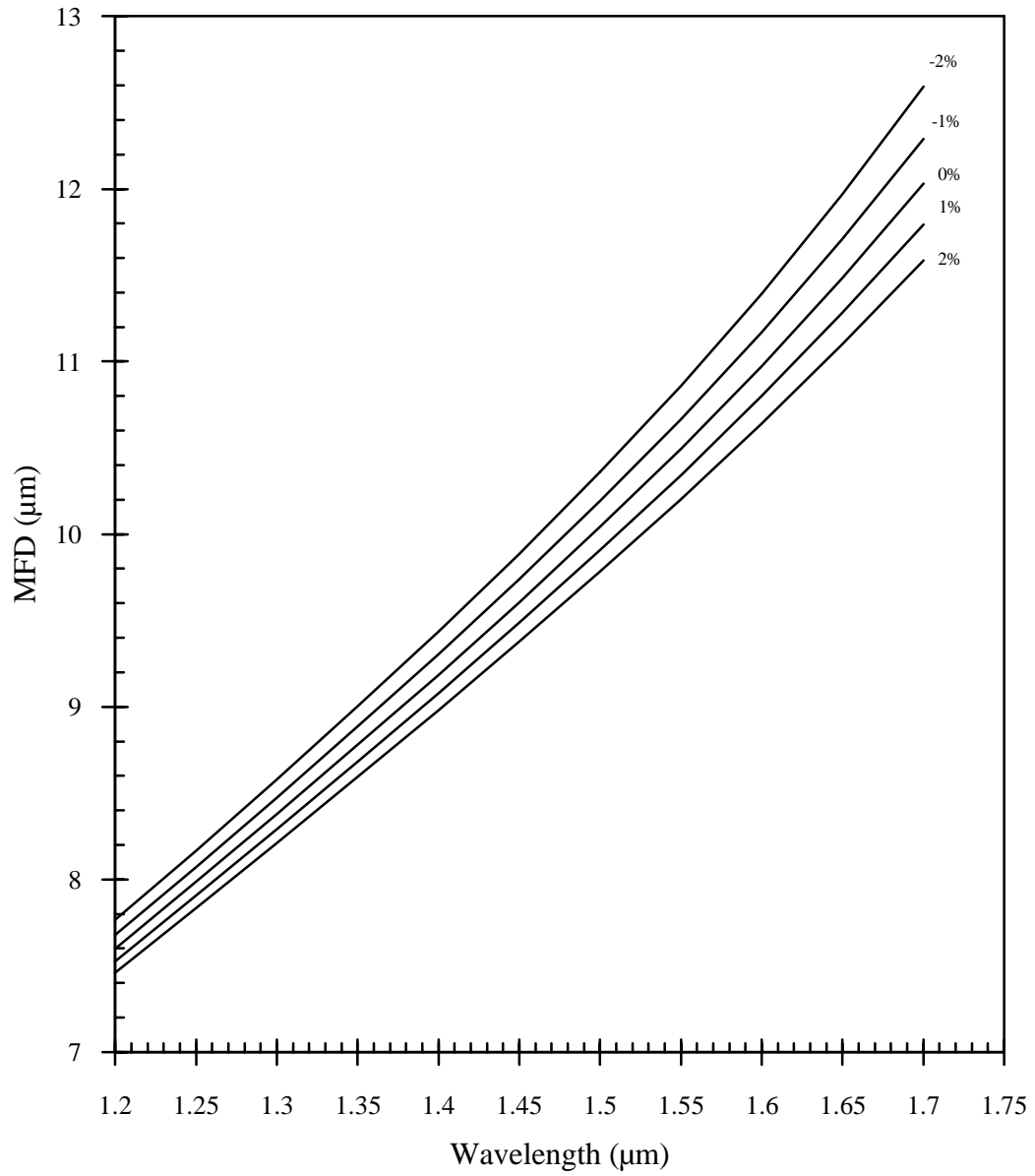


Figure 4.19 Variations of mode-field diameter versus wavelength of fundamental LP₀₁ mode for radius a_2 variations of $\pm 1\%$ and $\pm 2\%$.

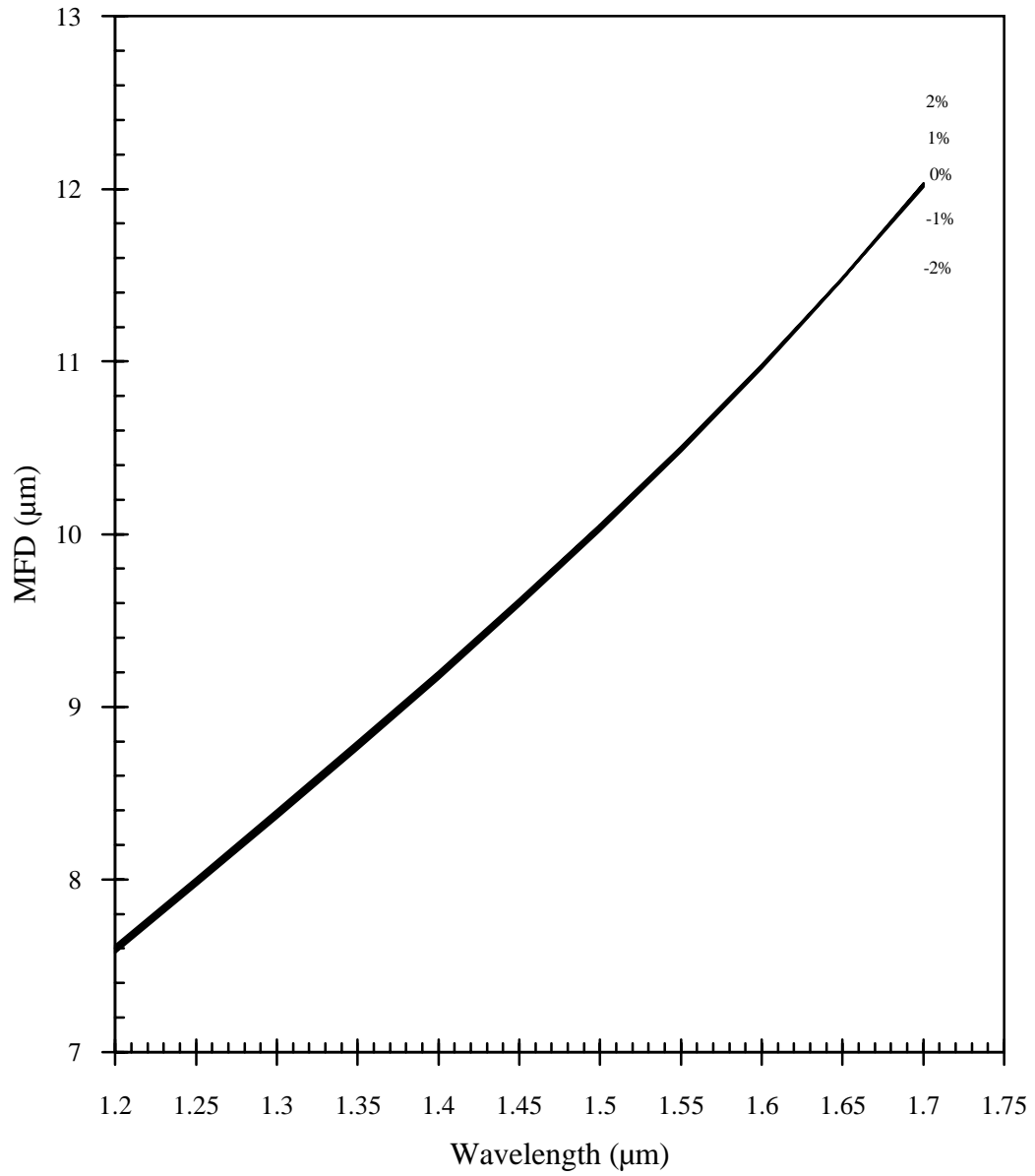


Figure 4.20 Variations of mode-field diameter versus wavelength of fundamental LP₀₁ mode for radius a_3 variations of $\pm 1\%$ and $\pm 2\%$.

Table 4.7 Mode-Field Diameter Values in μm At $\lambda = 1.55 \mu\text{m}$ As The Radius α_i ($i = 1, 2, \text{ and } 3$) Of The Fiber Changes.

Percent Variations of α_i	Mode-Field Diameter Due To Radius α_1 Changes	Mode-Field Diameter Due To Radius α_2 Changes	Mode-Field Diameter Due To Radius α_3 Changes
-2%	10.24	10.86	10.51
-1%	10.36	10.67	10.5
0%	10.5	10.5	10.5
1%	10.64	10.34	10.49
2%	10.78	10.2	10.48